Modeling impacts of nutrient loading, warming, and boundary exchanges on hypoxia and metabolism in a shallow estuarine ecosystem

Jeremy M. Testa, Nicole Basenback, Chunqi Shen, Kelly Cole, Amanda Moore, Casey Hodgkins, Damian C. Brady

Chesapeake Biological Laboratory (Testa, Shen, Moore, Hodgkins), University of Maryland Center for Environmental Science, Solomons, Maryland, USA; University of Maryland College of Agriculture and Natural Resources (Basenback), College Park, Maryland, USA; Civil and Environmental Engineering (Cole), University of Maine, Orono, Maine, USA; School of Marine Sciences (Brady), University of Maine, Walpole, Maine, USA
(Correspondence to Testa: jtesta@umces.edu)

Keywords: eutrophication < ECOLOGY, total maximum daily loading (TMDL) < WATER QUALITY, estuaries < GEOGRAPHY, Chesapeake Bay, Chester River estuary, climate variability/change < CLIMATE, Metabolism, biogeochemical model

Research Impact statement: Future warming will decrease net ecosystem metabolism and increase hypoxia in a small estuary, but warming and nutrient load effects on connected waterbodies will also be translated into the estuary.

Abstract

We sought to investigate the impacts of nutrient loading, warming, and open-water boundary exchanges on a shallow estuary through idealized numerical model experiments. We performed these simulations using a stand-alone implementation of the ROMS-RCA biogeochemical model in the Chester River estuary, a tributary estuary within the Chesapeake Bay estuarine complex. We found that metabolic rates were elevated in the shallow tributary creeks of the estuary relative to open waters, and that rates of gross primary production, respiration, and net ecosystem metabolism were a function of both water temperature and local phytoplankton biomass. Warming rates of 0.75 and 1.25ºC led to reductions in dissolved oxygen concentrations throughout the estuary. Reductions (50%) in dissolved nitrogen and phosphorus loading did not substantially alter hypoxic volumes in this turbid, nutrient-rich estuary, but warming increased hypoxic volumes by 20-30%. Alterations of the open-water boundary that represent improved oxygen concentrations in the adjacent Chesapeake Bay mainstem led to more substantial relief of hypoxia in model simulations than nutrient reductions (~50% reductions in hypoxia). These simulations reveal the complex interplay of watershed nutrient inputs and horizontal exchange in a small tributary estuary, including the finding that future warming and nutrient reduction effects on Chesapeake Bay hypoxia will be translated to tributary estuaries like the Chester River.

Introduction

Biogeochemical processes in coastal ecosystems are closely linked to adjacent land use, internal physical, biological, and chemical processes, and remote forcing from adjacent tidal waters. A key interaction within the Anthropocene is the alteration of watershed nutrient budgets and hydrology through urbanization and agricultural expansion and intensity combined with warming temperature and altered precipitation patterns. Elevated nutrient loading combined with warmer, wetter conditions in many temperate ecosystems is associated with enhanced oxygen depletion (Laurent, Fennel et al. 2018; Ni, Li et al. 2019), altered phytoplankton biomass (Boynton, Kemp et al. 1982), and pressures on macrophyte and benthic communities (Lefcheck, Wilcox et al. 2017). While the potential scope of biogeochemical changes associated with eutrophication and climate change is large, it remains a challenge to meaningfully predict future

changes given uncertainties in projected climate variability, the effects of climate on phytoplankton production and composition, and watershed dynamics (Wagena, Collick et al. 2018). This is especially true considering that climate will impart differential impacts on components of coupled human-watershed-estuarine systems via changes in hydrology (Neff, Chang et al. 2000), temperature (Altieri and Gedan 2015), solar radiation (Nixon, Fulweiler et al. 2009), and agricultural practices (Ortiz-Bobea, Wang et al. 2019).

Due to the nature of their bathymetry and proximity to land, shallow estuarine systems have several unique characteristics compared to larger, deeper systems. Whereas deep estuaries have production and respiration cycles dominated by water-column plankton (e.g., Fennel and Testa 2019), shallow estuaries can be dominated by benthic metabolism from submerged aquatic vegetation (Ganju, Testa et al. 2020), microphytobenthos (McGlathery, Sundbäck et al. 2007), or subtidal sediments. One consequence of this distinction is that oxygen depletion in deeper systems tends to be a seasonal, kilometer-scale phenomenon supported by sinking phytoplankton-derived organic material, while shallow ecosystems can generate local diel cycling hypoxia over 6-12 hours as a result of high rates of benthic metabolism or high rates of water-column respiration associated with high phytoplankton biomass (>100 μg/L; e.g., Tyler et al. 2009). In the case of Chesapeake Bay and other drowned river valleys, shallow tributary estuaries are also responsive to the influence of larger, adjacent water bodies where water exchange can lead to import of organic material (Smith 1991), high-nutrient or low-oxygen water into their lower reaches on seasonal or event-scales (L. P. Sanford & Boicourt, 1990; Testa, Kemp, Boynton, & Hagy, 2008), or poorly buffered upwelling water (Grantham, Chan et al. 2004).

Numerical models have been widely used to generate projections of future conditions in response to climate warming, precipitation (and freshwater input) changes, and nutrient abatement actions (Meier, Andersson et al. 2011; Irby, Friedrichs et al. 2018; Lajaunie-Salla, Sottolichio et al. 2018; Laurent, Fennel et al. 2018; Ni, Li et al. 2019). The rationale for using complex, three-dimensional numerical models to generate future projections is that they integrate the coupled biogeochemical-hydrodynamic interactions that will result from altered physical and chemical conditions. In particular, simulations quantify how climate changes (e.g., warming, elevated river flow) may make the achievement of water quality standards more difficult, resulting in adjusted allocations for nutrient reduction targets (Justíc, Turner et al. 2003; Irby,

Friedrichs et al. 2018). In general, these projections have been made for large, relatively deep coastal ecosystems where sophisticated numerical models had previously been developed (e.g., northern Gulf of Mexico, Baltic Sea, Chesapeake Bay, Salish Sea). Far fewer model projections have been made for very shallow coastal systems that fringe the land-sea interface (Lajaunie-Salla, Sottolichio et al. 2018), despite the fact that these shallow ecosystems are (1) likely to be highly sensitive to future climatic change, (2) locations if intense biogeochemical processing of watershed inputs, and (3) important areas for tourism, fisheries, and aquaculture.

The purpose of this paper is to use a three-dimensional coupled hydrodynamic-biogeochemical model to quantify the sensitivity of oxygen depletion and metabolism in a shallow estuary to elevated temperature, altered nutrient inputs, and oxygen conditions at the open-water boundary. We use the Chester River Estuary as an experimental system, as it includes both seasonal, deep water hypoxia and shallow water diel cycling hypoxia. We present sensitivity simulations over an annual cycle in the estuary, and address the spatial and temporal changes in hypoxia and the metabolic rate processes driving oxygen production and consumption.

Methods

To evaluate the sensitivity of low oxygen conditions in the Chester River estuary to altered external forcing, we conducted a series of idealized simulations using a coupled, three dimension hydrodynamic-biogeochemical model (Regional Ocean Modeling System-Row-Column AESOP). After validating the model with the best available data, we adjusted three main inputs to the model: (1) nutrient loading from 12 major freshwater sources, (2) factors related to warming from climate projections, and (3) oxygen conditions at the open-water boundary associated with potential changes in hypoxia in the mainstem of the Chesapeake Bay. We did not investigate the impacts of sea level rise or altered precipitation patterns, which are also expected to change in a future climate (Ni, Li et al. 2019). Model response metrics we quantified included ecosystem responses in terms of the volume, duration, and extent of hypoxic waters and rates of oxygen production and consumption in the water-column and sediments.

Study Site: The Chester River Estuary is located on the eastern shore of Maryland, a peninsula on the eastern fringe of the Chesapeake Bay (Fig. 1). The estuary has a maximum depth of approximately 18 meters in a deep channel in the lower estuary, but a majority of the estuary is

less than 6 meters deep (Fig. 1), especially in several sub-tributaries (e.g., Corsica River, Langford Creek, Southeast Creek; Fig. 2). The 1,140 km^2 watershed consists of predominantly agricultural land use (65%) and lies within the coastal plain. The estuary exchanges with the mainstem of Chesapeake Bay at its seaward open-water boundary and with Eastern Bay to the south through a narrow channel at Kent Narrows (Fig. 2).

Numerical Model and Data Sources: A coupled hydrodynamic-biogeochemical model was applied to simulate and analyze estuarine biogeochemical responses to simulated changes in nutrient input, temperature, and open-water boundary conditions. The hydrodynamic model is an application of the Regional Ocean Modeling System (ROMS) with a 174 x 174 grid that includes 200 meter horizontal resolution and 10 vertical layers, and is a stand-alone implementation that is not nested in a larger domain. Freshwater inputs to the estuary were delivered from 12 major rivers and creeks (Fig. 1, S1, S2) and derived from predictions from the Hydrologic Simulation Program Fortran (HSPF) as part of the Phase 6 Chesapeake Bay Program Watershed Model (Shenk, Wu et al. 2012). Atmospheric forcing for net heat flux, total downward radiation, precipitation, and evaporation were derived from the North American Regional Reanalysis (NARR; https://www.ncdc.noaa.gov/data-access/model-data/model-datasets/north-american-regional-reanalysis-narr) product. Wind forcing, air temperature, and barometric pressure were obtained from the Thomas Point buoy located near the Chester River (38.899 N, 76.436 W) and accessed from the National Data Buoy Center (http://www.ndbc.noaa.gov/station_page.php?station=tplm2). Open-water boundary conditions for salinity and water temperature were averaged from two stations in the mainstem Chesapeake Bay (CB3.2 and CB3.3E) monitored on a biweekly to monthly basis (Fig. 2). Sea level changes at the open-water boundary were obtained from the Chesapeake Bay Program Water Quality and Sediment Transport model (Cerco and Noel 2013). A quadratic stress is exerted at the bed, assuming that the bottom boundary layer is logarithmic over a roughness height of 1mm.

ROMS was coupled to a biogeochemical model (Row-Column AESOP; RCA) that has been described in detail in prior publications (Testa, Li et al. 2014; Ni, Li et al. 2019; Shen, Testa et al. 2019a). In short, RCA models state variables representing at least two phytoplankton groups (representing diatoms and dinoflagellates), labile and refractory pools of dissolved and particulate carbon, nitrogen, phosphorus, and silica, dissolved oxygen (hereafter O_2), and O_2-

consuming reduced solutes (CH_4, H_2S). RCA also includes a two-layer sediment module that includes an aerobic and anaerobic layer and represents deposition, remineralization, solute-sediment partitioning, burial, mixing, and biogeochemical reactions, such as sulfide and ammonium oxidation, and denitrification (Di Toro 2001; Brady, Testa et al. 2013; Testa, Brady et al. 2013). Initial conditions for water-column state variables were first derived from long-term monitoring stations (Fig. 2) and initial sediment conditions were extracted from ROMS-RCA simulations (dissolved constituents) previously simulated for Chesapeake Bay (Testa, Li et al. 2014; Shen, Testa et al. 2019a) and particulate carbon, nitrogen and phosphorus content from observations made in 2001 (Frank, Rohland et al. 2002). The model was then run for an annual cycle to allow for water-column and nutrient conditions to stabilize to locally-relevant conditions in the model simulation year 2003. Open-water boundary conditions were derived from the same monitoring stations as for salinity and temperature, and watershed loads of nutrients were derived from the Phase 6 simulation of the Chesapeake Bay Watershed Model.

Model Validation Data: The base 2003 model simulation was validated using bi-monthly to monthly, station-specific measurements of salinity, water temperature, chlorophyll-a, dissolved (DON, DOP, PO_4^{3-}, NO_2^-+NO_3^-, and NH_4^+) and particulate nutrient concentrations, and O_2 from the Chesapeake Bay Program (CBP) monitoring program (https://www.chesapeakebay.net) at several stations in the main estuarine channel (Fig. 2) and several additional stations along the shallow shoals (Fig. 2). High-frequency data from the Maryland Department of Natural Resources Continuous Monitoring (ConMon) program (http://eyesonthebay.dnr.maryland.gov/) were also used to validate the model, where salinity, temperature, and O_2 were measured. ConMon data are collected via a Xylem/YSI sonde containing multiple sensors sampling water properties (salinity, temperature, and O_2) every 15 minutes. Sondes are replaced with a newly calibrated instrument every two weeks and discrete water samples for chlorophyll-a, total suspended solids (TSS), nutrients, and particulate organic matter were collected at these times to post-calibrate sensors. We also compared simulated rates of sediment-water fluxes of nitrate (NO_{23}), ammonium (NH_4), phosphate (PO_4^3), and O_2 (sediment oxygen demand; SOD) using observations made at several stations during the summer of 2001 (June-August; Fig. S5) in intact sediment core incubations in the Chester and Corsica River estuaries (Boynton, Ceballos et al. 2018).

156 We used multiple model-data comparison metrics to assess the ability of the model to
157 simulate biogeochemical dynamics, including root mean square error (RMSE), mean error (ME),
158 and the reliability index (RI). Complete details and equations for the metrics can be found in
159 Stow, Jolliff et al. (2009) and Fitzpatrick (2009), but in brief, RMSE quantifies the magnitude of
160 overall model-data discrepancies, while ME indicates both the magnitude and direction of the
161 mean of model-data discrepancies. Both RMSE and ME are in the same units as the variable of
162 interest. The reliability index describes the average multiplicative difference between model
163 output and observations. For example, an RI of 2 would indicate that the model predicts the
164 observations within a factor of 2.
165
166 *Nutrient Reduction Scenarios:* We tested the sensitivity of Chester River O_2 concentrations to
167 changes in the overall magnitude of both nitrate and phosphate loading. Model scenarios
168 consisted of decreasing the nitrogen (NO_{23}, nitrate + nitrite) and phosphorus (PO_4)
169 concentrations in stream discharges for each of the 12 major rivers by 50%, where the decreases
170 were applied uniformly over the annual cycle. NO_{23} and PO_4 reduction scenarios were performed
171 independently, and we did not simulate simultaneous reductions of both nutrients. For
172 comparison, the total Chesapeake Bay TMDL includes a 19.1% reduction in TN and a 23.8%
173 reduction in TP from 2009 loads, while the Chester River Estuary includes a 17.4% reduction in
174 TN and a 9.8% reduction in TP from 2009 loads (CBP 2010). Here, we hypothesized that
175 nutrient load decreases will generate less extensive and shorter-duration hypoxic conditions in
176 main channel bottom waters via reduced phytoplankton production and deposition. We evaluated
177 changes in surface and bottom O_2 concentrations, estuarine volumes of hypoxic water (where
178 hypoxia was defined as < 5, 3.2, and 2 mg/L O_2 L^{-1} using O_2 criteria targets), and the duration of
179 O_2 concentrations less than the three specified O_2 thresholds.
180
181 *Elevated Temperature Scenarios:* We also performed idealized model scenarios of elevated water
182 temperature, where water temperatures were elevated by 0.75 and 1.25 ^oC in the biogeochemical
183 model simulation, applied uniformly to all estuarine cells and on all days within the annual cycle.
184 We did not simulate the hydrodynamic response to temperature by applying warming to the
185 atmospheric, riverine, or open-water boundaries. Recent analyses of Chesapeake water
186 temperature trends have suggested surface water warming of 0.5 to >2^oC over the past 30 years

(Ding and Elmore 2015) and projections of warming suggest increases of at least 1.5°C between the present day and the mid-century (Ni, Li et al. 2019). Given the well-described impacts of water temperature on solubility and metabolic rates (Yvon-Durocher, Caffrey et al. 2012; Breitburg, Levin et al. 2018), we quantified the vulnerability of O_2 conditions to future warming. We hypothesized that warming will reduce surface layer O_2 concentrations through reduced solubility, and reduce bottom-water O_2 through elevated respiration and reduced vertical mixing of oxygen.

Sensitivity of Dissolved Oxygen to the Chesapeake Bay Boundary: We simulated a scenario that represents improved oxygen concentrations in the open-water boundary that could be expected from watershed nutrient management in the broader Chesapeake Bay increasing O_2 concentrations at the open-water boundary of the Chester estuary. The lower Chester River estuary exchanges at its open-water boundary with the most severely O_2 depleted region of Chesapeake Bay (Testa and Kemp 2014), a region that is also vulnerable to future warming-induced hypoxia (Ni, Li et al. 2019). To examine the potential effects of advection or mixing of Chesapeake Bay waters on Chester River hypoxia, we adjusted the open-water O_2 boundary condition to represent reduced hypoxic conditions in lower layers of Chesapeake Bay. Here, we set bottom O_2 concentrations to those observed in 2001, a year with relatively high O_2 concentrations in the mainstem of Chesapeake Bay (Li, Lee et al. 2016).

Climatic Impacts on Gross Primary Production and Respiration: We used two approaches to assess the potential impacts of climate change on rates of gross primary production (GPP) and respiration. First, we post-processed the numerical model output to calculate water-column integrated rates of gross primary production and sediment+water column respiration rates at each hourly time-step. Water-column respiration rates include phytoplankton respiration, organic carbon oxidation, and oxidation of sulfide and methane, while sediment respiration rates include the sediment oxygen demand simulated within the sediment flux model module. Comparable approaches to estimating metabolism have been previously applied for ROMS-RCA in Chesapeake Bay (Testa, Li et al. 2014; Shen, Testa et al. 2019b).

Second, we estimated ecosystem gross primary production, respiration, and net ecosystem metabolism (NEM) from observed continuous (15-minute) time-series of O_2 at eight

218 locations (Fig. 2). The original concept and method for computing gross GPP and respiration
219 (and NEM) was developed in the 1950s (Odum and Hoskin 1958) and has subsequently been
220 modified for a variety of aquatic ecosystems (Caffrey 2004). The approach derives ecosystem
221 rates of gross primary production (P_g = GPP) and respiration (R_t) from increases in O_2
222 concentrations during daylight hours and declines during nighttime hours, respectively. The sum
223 of these two processes over 24 h, after correcting for air-sea exchange, provides an estimate of
224 NEM. We used continuous O_2 concentration measurements at eight locations in the Chester
225 River estuary from 2003 to 2016 (Fig. 2) to apply a modified approach (Beck, Hagy et al. 2015),
226 which uses a weighted regression to remove tidal effects on O_2 time-series since the tide can
227 advect higher or lower O_2 past the sensor thereby influencing the calculation of NEM. The
228 changes in O_2 used to compute metabolic rates were corrected for air-water gas exchange using
229 the equation $D = K_a (C_s\text{-}C)$, where D is the rate of air-water O_2 exchange (mg O_2 L^{-1} h^{-1}), K_a is
230 the volumetric aeration coefficient (h^{-1}), and C_s and C are the O_2 saturation concentration and
231 observed O_2 concentration (mg O_2 L^{-1}), respectively. K_a was computed as a function of wind
232 speed derived from the North American Land Data Assimilation System (NLDAS) and details of
233 the air-water gas calculation are incorporated into the R package WtRegDO (Beck, Hagy et al.
234 2015) and described in detail elsewhere (Thébault, Schraga et al. 2008). The calculations utilized
235 salinity, temperature, and O_2 times-series from the sensors at each platform, and atmospheric
236 pressure and air temperature data from the North American Regional Reanalysis (NARR). Tidal
237 height data were obtained from a nearby NOAA station at Tolchester Beach, Maryland
238 (https://tidesandcurrents.noaa.gov/waterlevels.html?id=8573364). The O_2 data used to make
239 metabolic computations were obtained from sensors deployed near-bottom in relatively shallow
240 waters (Table 2) that were well-mixed, which is necessary for the air-water flux correction to be
241 valid and for the O_2 time-series to be representative of the combined water-column and
242 sediments (Murrell, Caffrey et al. 2018).
243
244 **Results**
245 We present a validation of baseline biogeochemical model simulation against observed
246 concentrations and metabolic rates for key conditions in 2003, a year with relatively high
247 freshwater inputs year-round (Fig. 3). The seasonal cycle of hypoxia in the Chester River is
248 characterized by warm-season peaks, where the most spatially and temporally extensive O_2

depletion occurred near the mouth of the estuary (i.e. boundary adjacent to Chesapeake Bay) along the deepest part of the river channel (Fig.1). Deep channel hypoxia dominates the volume of low-O_2 water in the estuary and is highly influenced by exchange with near-anoxic waters at the open-water boundary with the mainstem of Chesapeake Bay. The results of idealized scenario simulations of (1) warming, (2) nutrient reductions, and (3) exchange of higher oxygen bottom water from the open boundary with Chesapeake Bay indicate that the extent of low-O_2 water was more sensitive to warming and exchanges with mainstem Chesapeake Bay bottom water O_2 than it was to reductions in watershed nitrogen and phosphorus inputs.

Water-Column Model Validation

Model simulations reasonably captured the observed seasonal variability in several key properties (i.e., water temperature, salinity, NO_{23}, NH_4, dissolved O_2, and PO_4) in most estuarine regions, but underestimated peak seasonal values for chl-a (ME < 0; Table 1, Fig. 4). Dissolved oxygen was well-represented by the model, with RI predominantly less than 1.3 and a seasonal O_2 cycle that mirrored water temperature, with mid-summer maxima in temperature and minima in bottom O_2 (Fig. 4). The RMSE for NO_{23} was low (generally < 0.5 mg L^{-1}) relative ambient concentrations, while NH_4 was typically over-estimated by the model (ME > 0; Table 1). NH_4 was elevated during warmer months in both the modeled and observed surface values in the upper and middle reaches of the estuary. In 2003, freshwater discharge into the Chester River was characterized by several 3-4 week periods of elevated flow, with peaks during March, June, and November-December (Fig. 3). Consequently, there was not a clear seasonal cycle in modeled or measured nutrient concentrations, outside of a winter peak in NO_{23} and PO_4, and modeled PO_4 concentrations were generally lower than those observed (ME < 0, RI ~3) . There was a clear spring bloom peak in chl-a in the lower reaches of the estuary, with modeled and observed values reaching peaks between 40 and 60 μg/L (Fig. 4), but model-simulated surface chl-a was lower than observed (ME <0, RI= 2.2; Table 1).

Ecosystem Metabolism Dynamics and Validation

Estimates of P_g (GPP), R_t, and NEM from observed O_2 time series were highly correlated with temperature on a seasonal basis, but the magnitude of rates varied spatially with differences in chlorophyll-a (Figs. 5&6). May-October mean values of respiration, for example, ranged from

50-250 mmol O_2 m^{-2} d^{-1} (~1.6-8 g O_2 m^{-2} d^{-1}) over the years of record, and were elevated within the sub tributary stations of the Corsica River (The Sill, Sycamore Point, Possum Point, Emory Creek) relative to the two stations in the main body of the Chester (Rolph's Wharf, Deep landing; Figs. 2&5). Median measured chlorophyll-a concentrations at the Corsica River stations were 13.8-36.3 μg/L, which were 50% higher than chlorophyll-a concentrations measured over a similar period in the adjacent Chester River (6.3-12.5 μg/L; Table S3). Respiration rates at a given temperature were higher under conditions of elevated chlorophyll within stations (Fig. 6). For the two stations located within a small inlet in the lower Chester River estuary (Kent Narrows 'Inside' and 'Outside'; Fig. 2), computed respiration rates were a factor of two larger at the inner, more protected station than the outer station (Fig. 5). As a consequence, the temperature-respiration slope was 2.5 times higher in the inner station than the outer station (Fig. 6). Despite these spatial differences, rates of Rt were significantly correlated with temperature at all sites, but with lower slopes in the main Chester channel region (Fig. 6). Regressions of Rt versus temperature reveal that mean slopes of -8 mmol O_2 m^{-2} d^{-1} $°C^{-1}$ and -14.1 mmol O_2 m^{-2} d^{-1} $°C^{-1}$ for the Chester River estuary and Corsica River estuary, respectively. Rates of NEM were predominantly negative across all stations in the estuary and NEM was negatively correlated with temperature (i.e., more heterotrophy with higher temperatures) at all but one of the Chester River stations analyzed, with slopes ranging from 0.41 to -1.05 mmol O_2 m^{-2} d^{-1} (Fig. S6).

Warming Impacts on Dissolved Oxygen and Metabolic Rates

Warming scenarios with elevated water temperatures of 0.75 and 1.25 °C relative to 2003 conditions predicted lower surface and bottom O_2 concentrations (Fig. 7). In both surface and bottom waters, O_2 concentrations were lowered by 0.1 to 0.2 mg O_2 L^{-1} under a 0.75 °C warming and by 0.1 to 0.8 mg O_2 L^{-1} in the 1.25 °C warming scenario (Fig. 7). The declines in O_2 in response to warming were highest during the March to August period, except during a period between days 160 and 190 (mid-June to mid-July) where riverine inputs were high (Fig. 3) and between days 210 and 225 (early August) where an influx of high O_2 water from mainstem Chesapeake Bay offset O_2 reductions due to warming (Fig. 7). Depending on the season, the percentage decrease in O_2 concentrations ranged from 4% during spring and up to 7% during summer under the 1.25 °C warming scenario (Fig. 7). We also controlled for the impacts of

temperature by examining changes in solubility associated with a 1.25 °C warming at surface pressure and a salinity of 7, and found that O_2 declines above 0.3 mg O_2 L^{-1} exceed that expected from solubility changes, which were simulated for spring and late summer periods (Fig. 7).

We also quantified changes in estuary-wide volumes of low-O_2 water resulting from warming, and considered volumes with O_2 concentrations less than 5, 3.2, and 2 mg O_2 L^{-1}, which correspond with O_2 criteria used in Chesapeake Bay water quality management (Zhang, Tango et al. 2018). The volumes of all low- O_2 waters increased with warming, and the volume expansions per rate of warming (ΔVolume/Δ^oC) were similar across the two warming scenarios, as were the relative size of the volume expansion relative to base conditions (5-7% increase). There were little differences in low O_2 volumes among the scenarios during the August oxygenation event associated with Chesapeake Bay boundary water influx, except for the 5 mg O_2 L^{-1} threshold where volumes increase by 2-3% (Fig. 8).

Warming also altered ecosystem metabolic rates in the Chester River, leading to increases in NEM during cool seasons and declines in NEM in warm seasons (Fig. 9). In the middle region of the estuary (Station XIH0077), warming led to elevated winter-spring gross primary production (GPP, which is equivalent to the observation-based P_g) by 20-120% during February to March, and reduced GPP during mid-summer (17-41% decrease from July to September) under 1.25 °C warming (Fig. 9). Respiration under warming also had a seasonally-dependent response, with increases in respiration (1-14 % under 1.25 °C warming) in all months except the periods where transitions in phytoplankton groups occurred, including April-May, and September and November (Fig. 9). The warm-season respiration amplification and GPP reductions during spring and fall months under warming led to enhancement of net heterotrophic conditions (increasingly negative NEM) in nearly all months of the year, except during February-March (Fig. 9). The relative decrease in NEM was proportionally larger than the changes in GPP and respiration under warming, revealing the multiplicative effects of lower GPP and elevated respiration.

Nitrogen and Phosphorus Reduction Scenarios

At the estuary scale, the idealized simulations with 50% reductions in nitrate (NO_{23}) and phosphate (PO_4) loading resulted in only marginal changes in the three thresholds of hypoxic volume (Fig. S4), but revealed that P limitation is more important than N limitation. For

example, rates of modeled GPP and respiration were reduced by 6-18% (GPP) and 1-9% (respiration) during the May-October period in the PO_4 load reduction scenarios and unaffected by changes in NO_{23} loads (Fig. 10). Correspondingly, PO_4 reductions caused a decrease in hypoxic volume of 1-1.5% relative to the Base (no change) scenario, with a comparably minor increase in response to NO_{23} reductions.

Dissolved Oxygen at the Chesapeake Bay Boundary Scenario

Scenarios that included elevated O_2 at the Chesapeake Bay boundary had a larger effect on the hypoxic volume within the Chester River than watershed nutrient load reductions or temperature increases. By increasing the O_2 in the sub-surface layers of the boundary domain at a level consistent with recently observed "best-case' scenarios in Chesapeake Bay (year 2001), the total hypoxic volume between June and September decreased by a range of 7-55% at the threshold of 2 mg O_2 L^{-1}), 4-40% for the 3.2 mg O_2 L^{-1} threshold, and 4-30% at the 5 mg O_2 L^{-1} threshold (Fig. 11; Table S4). These boundary-exchange effects were largest in absolute terms during late summer hypoxic periods, but were also substantial during the lower volume periods (August, October; Table S4). We did not examine the impacts of sea level changes or examine fine temporal-scale variations associated with tidal mixing.

Discussion

We used data-derived estimates of metabolic rates and numerical model simulations of future warming scenarios to examine the sensitivity of a shallow estuarine ecosystem to future warming. Results indicate that warming will elevate respiration rates and associated O_2 consumption, but the magnitude of the temperature-dependency of respiration is positively correlated with local productivity. Warming reduced O_2 concentrations throughout the estuary, with contributions from reduced solubility generally exceeding those from elevated respiration outside of spring and late-summer periods. This particular estuary, which is turbid and nutrient-rich, was relatively insensitive to relatively large (50%) local watershed nutrient reductions. In contrast, relatively small increases in O_2 in open-water boundary reduced overall hypoxia in the estuary, highlighting the influence of Chesapeake Bay hypoxia on Chester River hypoxia and thus the need for watershed-scale nutrient reductions to address local tributary O_2 conditions.

Temperature is a primary driver of ecosystem primary production (GPP, or P_g), respiration (R_t), and NEM based on analyses of recent continuous O_2 records (2003-2017) and model simulations in the Chester River estuary. Temperature is often cited as primary driver of metabolic rate processes across ecosystems (Yvon-Durocher, Caffrey et al. 2012; Caffrey, Murrell et al. 2014), supporting predictions and assertions that future warming should elevate respiration rates and O_2 depletion (Carstensen, Andersen et al. 2014; Breitburg, Levin et al. 2018; Ni, Li et al. 2019), but the net balance between temperature-effects on GPP and R_t ultimately controls oxygen responses. Observation-derived NEM in the Chester estuary was negatively correlated with temperature (Fig. S6), consistent with model scenarios that suggest future warming will enhance net heterotrophy and further contribute to low O_2 concentrations. This is consistent with predictions of increasing net heterotophy in a warmer future climate, which in part derive from predictions of a higher sensitivity of respiration to temperature than photosynthesis (Yvon-Durocher, Jones et al. 2010). However, modeling studies in other Chesapeake Bay tributaries suggest a more complex picture. For example, Lake and Brush (2015) found that warming increased net primary production (NPP) in upper estuarine regions due to enhanced nutrient remineralization, but reduced NPP in down-estuary regions during summer. Tassone and Bukaveckas (2019) found rates of metabolism in the James River estuary (e.g., median NEM ~ ±2 g O_2 m^{-2} d^{-1}) that were similar to our estimates in the Chester River (Fig. S6), but they also reported clear spatial patterns in metabolic rates that might suggest that internal spatial controls on NEM might lead to a varying response of NEM to warming.

NEM responses to warming are complicated by the fact that GPP and R_t tend to be highly correlated, given that organic matter generated by GPP fuels R_t. In the Chester River estuary, the increase in respiration rate in response to warming (e.g., the slope of R_t versus ^oC regressions) varied by a factor of 3 across stations, where the temperature sensitivity of R_t within protected, productive (e.g., high chlorophyll-*a*, high GPP) waters (slopes = -10.2 to -17.6) was much higher relative to more open, less productive waters (slopes = -5.44 to -7.57). Thus, respiration-derived increases in O_2 consumption in response to future warming will be a function of spatially variable, local productivity and organic matter availability (Testa and Kemp 2008; Lake and Brush 2015). As a consequence, eutrophication abatement and associated productivity declines may allow for increased resilience to warming if associated respiration rates in underlying deep waters or during night are reduced (Irby, Friedrichs et al. 2018; Laurent, Fennel

et al. 2018). Our model simulations indicated that GPP declined in response to warming during some seasons (as temperature exceeded optimal phytoplankton growth rates), while GPP derived from oxygen time series was positively correlated with temperature, with slopes ranging from 5.13 to 16.5 mmol O_2 m^{-2} d^{-1}. Given the flexible and dynamic nature of phytoplankton communities in response to environmental change, however, such GPP reductions in response to warming may not emerge if species shift to organisms that grow at maximal rates under warming temperatures or if warming-induced nutrient remineralization stimulates additional GPP (e.g., Lake and Brush 2015). Given the complex nature of plankton food web responses to warming (Murphy, Romanuk et al. 2020), the ability of the simple phytoplankton models used in this analysis to predict future change is limited. Nevertheless, the fact that modeled R_t declined with lower GPP reinforces the strong dependency of these two metabolic indices and their impact on NEM.

The implementation of ROMS-RCA presented here did not include metabolic contributions of benthic primary producers (microalgae, submerged vascular plants; SAV) or exchange with fringing wetland communities, which could have influenced overall metabolic responses to simulated warming. Several prior investigations in nearby Chesapeake Bay tributaries (York River, James River) have indicated that benthic contributions to ecosystem metabolism can be substantial (Bukaveckas, Barry et al. 2011; Qin and Shen 2019). Modeled rates of GPP and respiration were generally lower than those derived from observed oxygen time-series (Fig. 9), which may reflect the omission of these important communities. Annual surveys of SAV coverage did not, however, indicate substantial cover of these vascular plants in any region of the Chester River in 2003 (VIMS 2020), suggesting that omission of SAV did not influence model outcomes. Although benthic microalgal communities can be important components of estuarine metabolism in shallow, clear water environments (Miller, Geider et al. 1996), typical values of light attenuation in the Chester estuary (mean k_{dPAR} = 3 m^{-1}) would only allow 1% of surface light to reach sediments at depths shallower than 1.5 m. Given that much higher light levels would be required to allow photosynthetic rates to substantially impact metabolism, the contributions of benthic microalgae in 2003 were likely to be small. This does not mean that benthic respiration is small in the Chester River, as measured rates of sediment oxygen uptake (~30 mmol O_2 m^{-2} d^{-1} or 0.95 g O_2 m^{-2} d^{-1}) are a substantial portion of ecosystem respiration (Fig. 9). Tidal exchange between estuaries and fringing tidal wetlands can also serve

to supplement estuarine organic matter stocks to support additional respiration (Cai 2011), but we do not have reliable estimates of tidal wetland exchange in the Chester estuary to assess the potential impact on modeled metabolism of omitting exchanges with tidal marshes. In the York River Estuary, it has been shown that respiration increases with warming given import of dissolved organic carbon from adjacent habitats (Lake and Brush 2015), suggesting that significant organic matter export could impact metabolic rates in this system.

Warming clearly reduced O_2 concentrations and led to elevated low-O_2 volumes and the magnitude of this response was seasonally-specific. Warming of 0.75 and 1.25 °C from current conditions led to elevated low O_2 volumes at all three threshold values by between 5 and 10%, suggesting incremental declines in O_2 with continued warming. This is consistent with model simulations in the York River estuary (Lake and Brush 2015), who also reported that hypoxia was more sensitive to warming in seaward estuarine regions. Prior projections of future warming effects in Chesapeake Bay mainstem waters indicated that water temperature was a dominant driver of hypoxic volume, with expected mid-21st century warming expected to cause 10-30% increases in low O_2 volumes (Irby, Friedrichs et al. 2018; Ni, Li et al. 2019). Hindcast simulations in Chesapeake Bay (1985 to the present) suggest that contemporary warming has already occurred (~0.8-1.5 °C) and was a stronger control on O_2 than modest reductions (10-15%) in nutrient loading (Ni, Li et al. 2020). Warming has also been implicated in expanded low O_2 waters in many estuaries and coastal seas (Justíc, Rabalais et al. 1996; Carstensen, Andersen et al. 2014; Breitburg, Levin et al. 2018; Laurent, Fennel et al. 2018). Although most of these studies examined changes in the volume of extensive hypoxic zones integrated over long time scales (e.g., decades), our results suggest that the impact of warming varies intra-annually, with more expansive increases under periods of high biological productivity and lower external influence from riverine or seaward boundaries. Our results also indicate that daily minima in O_2 are lower under warming (Fig. S3), which could lengthen the daily duration of diel cycling hypoxia in this system and other nearby shallow estuaries (Tyler, Brady et al. 2009).

Our idealized model simulations show that while Chester River O_2 dynamics are sensitive to changes in nutrient inputs, this sensitivity is far less than that of the adjacent mainstem Chesapeake Bay and other coastal water bodies (Laurent, Fennel et al. 2018; Wang, Hu et al. 2018; Irby and Friedrichs 2019). Low sensitivity to nutrient inputs is likely the result of high turbidity within this shallower, well-mixed system. Light attenuation coefficients (k_d) of 2 - 7 m^{-1}

(Fig. S2) far exceed those typically observed (< 1 m^{-1}) in the mainstem of Chesapeake Bay (Harding, Gallegos et al. 2015). These conditions imply light limitation for phytoplankton growth that is typical for these turbid, low salinity waters (Fisher et al., 1992). Analysis of modeled light limitation factors in ROMS-RCA (RLGHT), which vary between 0 and 1 and where 1 = no light limitation (Testa, Li et al. 2014), reveal that RLGHT was less than 0.5 for ~25% of the daytime simulation period at upstream and mid-Chester stations compared to ~5% at ET4.2, the most downstream station near the Chesapeake Bay mainstem. Thus, phytoplankton potential growth rates would be less than 50% of maximal rates in surface waters over much of the estuarine body for a substantial portion of the annual cycle. This is consistent with observations of spatial patterns of light availability in the Chester estuary, where total suspended solids (TSS) and Secchi depth data indicate more substantially light limited conditions in upstream regions, where higher TSS (20 - 25 mg L^{-1}), lower Secchi depths (0.2 - 0.4 m), and higher k_d (3 - 5 m^{-1}) were reported relative to the lower estuary with TSS of 5 - 10 mg L^{-1}, Secchi depth of 0.5-1.2 m, and k_d of 1-3 m^{-1}.

Another important factor leading to low sensitivity to nutrient inputs is the high ambient nutrient concentrations in the Chester River estuary. The Chester River has high nitrogen and phosphorus concentrations relative to 0.07 mg N L^{-1} and 0.007 mg P L^{-1} (Fig. 4), the levels generally considered by local water management targets as concentrations above which phytoplankton growth will not be stimulated by additional nutrient inputs (Zhang, Fisher et al. 2020). Observed NO_{23} and PO_4 concentrations were typically greater than 0.25 mg N L^{-1} and 0.01 mg P L^{-1} at Chester River stations (Fig 4), much higher than the half saturation coefficients in ROMS-RCA (0.01 mg N L^{-1} and 0.001 mg P L^{-1}). The ratio of phosphorus (PO_4), nitrogen (NO_{23}+NH_4), and silica concentrations to their respective half-saturation coefficients indicated that at both the upstream and downstream stations, none of the above nutrients were limiting, except for phosphorus during a brief period during winter-spring (i.e., ratios greater than 1, data not shown), during which GPP was reduced by PO_4 load reductions scenarios (Fig. 10). Tian (2020) recently reported that nutrient loading was an important factor controlling hypoxia in the Chester River using a multi-year numerical model simulation, but the reported half saturation coefficients for nitrogen and phosphorus uptake (0.5 mg N L^{-1} and 0.0025 mg P L^{-1}) were much larger than those used in other Chesapeake water quality models (e.g., 0.007-0.025 mg N/L) (Testa, Li et al. 2014; Feng, Friedrichs et al. 2015; Cerco and Noel 2017). This clearly indicates

that modest alterations in nutrient loading rates may be expected to have a much more limited impact on phytoplankton growth and hypoxia than the mainstem Chesapeake Bay and other nutrient-limited estuaries.

Of the local nutrient management scenarios we examined, phosphate (PO_4) loading reduction scenarios had a larger effect on metabolic rates and reductions in hypoxic volume than nitrogen reductions. This is consistent with low-salinity waters (the Chester River estuary mean salinity is < 10; Table 2) being more often phosphorus limited (Fisher, Peele et al. 1992; Jordan, Cornwell et al. 2008) than more seaward, higher-salinity waters. The effect of phosphorus load changes on the Chester River compared to nitrogen is the opposite effect to that observed in the Bay mainstem, where hypoxia is more sensitive to nitrogen loads (Testa et al., 2014). While our analysis revealed that Chester river nutrient concentrations are often above those limiting to phytoplankton growth, there are large regions of Chesapeake Bay vulnerable to nitrogen limitation (Kemp, Boynton et al. 2005). Complex spatial responses to alterations of phosphorus and nitrogen loading have been reported in other costal systems, where phosphorus declines were linked to less productivity in low-salinity waters, allowing for more nitrogen transport to support N-limited phytoplankton growth downstream (Laurent and Fennel 2014). Tradeoffs in N versus P limitation have been linked to spatially-dependent long-term changes in phytoplankton biomass in the Neuse River estuary (Paerl, Valdes et al. 2004), but we did not find a strong change in downstream phytoplankton biomass (or hypoxia) in response to P reductions.

Hypoxia was present seasonally in both deep and shallow waters (i.e., Corsica River), but the volume was dominated by deep water (i.e., >10 m) in the lower estuary. Hypoxic volumes have not been previously reported for the Chester River estuary and unsurprisingly, these simulations suggest that volumes < 2 mg O_2 L^{-1} of 0.1-1 km^3 are an order of magnitude smaller than mainstem Bay hypoxic volumes (2-15 km^3) (Murphy, Kemp et al. 2011; Irby, Friedrichs et al. 2016; Testa, Murphy et al. 2018). The deeper, stratified waters in the lower Chester River estuary appear to be strongly affected by low- O_2 waters encroaching from the adjacent Chesapeake Bay. In the 2003 simulations, bottom water O_2 concentrations increased and hypoxic volume declined in August during a period where wind speed was weak (Fig. 3; indicating no strong mixing). Simultaneously, O_2 concentrations at stations just outside the lower Chester River increased, indicating that cross-boundary exchange was a key factor driving Chester River hypoxia. Similarly, sensitivity simulations using boundary conditions with higher bottom O_2

conditions in Chesapeake Bay (2001) relieved hypoxia in the Chester River estuary by 4-55% (Table S4). In prior simulations of the Chester estuary, removing hypoxic concentrations completely from the open-water boundary reduced Chester River hypoxic volume by >90% (Basenback 2019). These results highlight that hypoxia in the Chester River is more sensitive to exchange with Chesapeake Bay than to local watershed nutrient inputs, and reinforces that larger-scale regional improvements in O_2 will be communicated to waters connected to the main stem Chesapeake volume. Furthermore, increases in hypoxia in the mainstem Chesapeake Bay associated with warming (Irby, Friedrichs et al. 2018; Ni, Li et al. 2019) would thus be expected to support additional hypoxia in the Chester River estuary given this boundary exchange, and thus our estimates of enhanced Chester River hypoxia under warming may be conservative.

A key response of shallow, highly productive ecosystems to warming and nutrient load reductions is the alteration of daily extremes in oxygen conditions. Diel-cycling hypoxia and other features of high oxygen variability have been reported in the Corsica River estuary, a small tributary of the Chester River (Boynton, Testa et al. 2009), as well as a wide-variety of coastal and freshwater ecosystems under conditions of eutrophication (D'Avanzo and Kremer 1994; Tyler, Brady et al. 2009), algal blooms (Hitchcock, Kirkpatrick et al. 2014), or dense vegetation cover (Andersen, Kragh et al. 2017). At a station in the Chester River estuary where 15-minute O_2 data were available in 2003, hourly O_2 variations were substantial (hourly standard deviation occasionally > 2 mg O_2 L^{-1}; Fig. 12) and during two events led to O_2 departures below 4 mg O_2 L^{-1} for several hours. Model-simulated O_2 did capture episodic variations outside of the annual seasonal cycle, but the short-term variations (~ hourly) were not as large (~0.1 mg O_2 L^{-1}) as observed (Fig. 12). The implication of this underestimation of diel-variability is that modeled metabolic rates were likely lower than observed (Fig. 9). However, warming scenarios led to clear downward departures in daily O_2 minima (Fig. S3), suggesting that warming will lead to not only reductions in mean O_2 but also increases in the duration of diel-cycling hypoxia. Future work should more fully address what is necessary to simulate diel hypoxia cycling, which may including increasing the spatial resolution to adequately capture the small scale hydrodynamics and associated residence time needed to allow for O_2 to decline and phytoplankton to reach elevated concentrations (e.g., > 100 mg m^{-3}) in the Corsica River estuary. Even the 200-meter horizontal resolution used in this model, which is substantially higher than models used for the mainstem of Chesapeake Bay (Testa, Li et al. 2014; Feng, Friedrichs et al. 2015) and other

coastal ecosystems (Fennel, Hu et al. 2013), was insufficient to capture these key dynamics in the Chester estuary.

Increased model resolution may also be necessary to better capture the biogeochemical dynamics that drive metabolic responses to long-term change. For example, while model-simulated rates of NEM were favorably comparable to estimates derived from dissolved oxygen time-series, model estimates of GPP and respiration appear to be lower than those estimated from observations (Fig. 9). Model-simulated chlorophyll-a was consistently lower than observed values in the middle regions of the estuary (ME<0; Table 1), supporting the idea that overall productivity was higher than simulated in 2003. Model underestimation of productivity does not appear to be linked to insufficient nutrient availability, given that the model reasonably captures dissolved nitrogen and phosphorus dynamics (Fig. 3) and the nutrient concentrations are not at limiting levels (as discussed above). Finer resolution (<100 m) hydrodynamic simulations have shown a diversity of eddy-like circulation patterns in the Chester River estuary that may locally enhance residence time and allow for more extensive phytoplankton blooms. If we assume that the model did underestimate metabolic rates, our simulated metabolic sensitivity to warming would likely be conservative and future, higher-resolution simulations would allow a test of this hypotheses.

Conclusions and Future Recommendations

Our study of O_2 dynamics and metabolic rate processes in response to temperature changes, nutrient load reductions, and boundary conditions reinforces the important role that warming has and will play in regulating water quality dynamics in estuarine ecosystems. Warming will make local management of eutrophic shallow estuaries more difficult due to the multiple reinforcing ecosystem rates (primary production, respiration, nutrient cycling) that temperature influences. In the Chester River estuary, the role of temperature was particularly relevant because the light-limited and nutrient-saturated nature of the system make it relatively insensitive to changes in watershed nutrient inputs, leading to temperature causing reduced NEM and enhanced heterotrophy. Furthermore, the dominant role of exchange with mainstem Chesapeake Bay waters in driving Chester River hypoxia demands further analysis of the role of tidal mixing, event-scale, and seasonal Chester-Chesapeake interactions. The boundary effect also reveals that long-term changes in connected estuarine systems are inherently linked (Testa,

588 Kemp et al. 2008) and that the impacts of nutrient reductions and warming on mainstem
589 Chesapeake hypoxia will be communicated to the Chester estuary to enhance or mitigate local
590 warming effects on O_2 concentrations. Despite the fact that the Chester River estuary was
591 relatively insensitive to local nutrient reductions, regional nutrient reductions that improve
592 mainstem Chesapeake Bay oxygen concentrations will provide benefits to the Chester estuary
593 and other tributary estuaries, while local reductions in the Chester River watershed will reduce
594 export through the Chester to the mainstem Bay.
595 Our results also reinforce that currently-established targets for nutrient load reductions
596 aimed at increasing O_2 concentrations may not be sufficient to achieve future oxygen targets
597 given expected warming (Irby, Friedrichs et al. 2018; Ni, Li et al. 2019; Ni, Li et al. 2020).
598 Adjustments to these nutrient targets, namely the Total Daily Maximum Load (TMDL), may be
599 necessary to overcome downward-moving targets for O_2 resulting from warming. Emerging
600 technologies have also been proposed to find engineered solutions to low O_2 conditions (Harris,
601 Hodgkins et al. 2015; Koweek, García-Sánchez et al. 2020), but the efficacy of these approaches
602 in larger systems remains unclear (Conley, Bonsdorff et al. 2009).
603 While we quantified the impacts of climate warming on the Chester River estuary,
604 warming is only one of several future changes predicted to emerge from global climate changes.
605 In Chesapeake Bay, altered magnitude and seasonality of precipitation and sea level rise are also
606 projected to change, and the hydrodynamic response to these forces will have diverse and
607 interactive impacts on circulation, phytoplankton productivity, and hypoxia (Irby, Friedrichs et
608 al. 2018; Ni, Li et al. 2019). Our analysis also focused on a single year (2003, hydrologically
609 moderately wet), thus to test how future warming may impact systems like the Chester River,
610 future work should include more hydrologic variability (i.e. very wet and dry) and specific
611 simulations of altered freshwater inputs that allow for an understanding of the range of physical
612 variations that could modulate hypoxia responses to warming. This could be especially important
613 in agriculturally dominated watersheds, where climate change will also impact watershed
614 nutrient processing, hydrology, and agriculture conservation practices (Wagena & Easton, 2018),
615 farmer adaptations to climate change (Chang, 2019; Huttunen et al., 2015), and watershed
616 restoration practices that influence sediment load (Palinkas, 2013). Ultimately, water quality
617 managers may need to assess optimal strategies in light of sensitivity to warming, changes in

hydrological patterns, and tidal boundary conditions, all of which may significantly decrease the efficacy of local watershed management practices.

Additional supporting information may be found online under the Supporting Information tab for this article: Included in the Supporting Information is additional statistics on watershed inputs, water properties at monitoring station, and additional model output and validation analyses.

Acknowledgements

We would like to dedicate this paper to the memory of James Fitzpatrick, who was instrumental in our original efforts to apply ROMS-RCA in Chesapeake Bay. A cherished friend and mentor, Jim generously offered his time and energy to our work and we will miss the many discussions he stimulated through his wit and curiosity. We would also like the thank the many state and federal agencies who collected and processed the datasets used in this analysis, including the Maryland Department of Natural Resources, the US EPA Chesapeake Bay Program, and the Maryland Department of the Environment. This work was supported by grants from the US Environmental Protection Agency (EPA-R3-CBP-14-02, CB96343601-EPASYNTH-19) and the National Science Foundation (CBET-13606395). This is the University of Maryland Publication #XXXX and CBL Technical Series CBXX-XXX.

Literature Cited

Altieri, A. H. and K. B. Gedan, 2015. Climate change and dead zones. *Global Change Biology* **21**:1395-1406.

Andersen, M. R., T. Kragh and K. Sand-Jensen, 2017. Extreme diel dissolved oxygen and carbon cycles in shallow vegetated lakes. *Proceedings of the Royal Society B: Biological Sciences* **284**:20171427.

Basenback, N., 2019. Phenology of estuarine response to anthropogenic and climatic drivers, a study of the Chesapeake Bay and Chester River Estuaries, Masters Thesis, University of Maryland.

Beck, M. W., J. D. Hagy and M. C. Murrell, 2015. Improving estimates of ecosystem metabolism by reducing effects of tidal advection on dissolved oxygen time series. *Limnology and Oceanography: Methods* **13**:731-745.

Boynton, W. R., M. A. C. Ceballos, E. M. Bailey, C. L. S. Hodgkins, J. L. Humphrey and J. M. Testa, 2018. Oxygen and Nutrient Exchanges at the Sediment-Water Interface: a Global Synthesis and Critique of Estuarine and Coastal Data. *Estuaries and Coasts* **41**:301-333.

Boynton, W. R., W. M. Kemp and C. W. Keefe, 1982. A comparative analysis of nutrients and other factors influencing estuarine phytoplankton production. *In*: *Estuarine Comparisons,* V. S. Kennedy (V. S. Kennedy)V. S. Kennedys). Academic Press, New York., pp. 69-90.

Boynton, W. R., J. M. Testa and W. M. Kemp, 2009. An Ecological Assessment of the Corsica River Estuary and Watershed Scientific Advice for Future Water Quality Management. *In: Final Report to Maryland Department of Natural Resource,* Editor (Editor)^(Editors).

Brady, D. C., J. M. Testa, D. M. Di Toro, W. R. Boynton and W. M. Kemp, 2013. Sediment flux modeling: calibration and application for coastal systems. *Estuarine, Coastal and Shelf Science* **117**:107-124.

Breitburg, D. L., L. A. Levin, A. Oschlies, M. Grégoire, F. P. Chavez, D. J. Conley, V. Garçon, D. Gilbert, D. Gutiérrez, K. Isensee, G. S. Jacinto, K. E. Limburg, I. Montes, S. W. A. Naqvi, G. C. Pitcher, N. N. Rabalais, M. R. Roman, K. A. Rose, B. A. Seibel, M. Telszewski, M. Yasuhara and J. Zhang, 2018. Declining oxygen in the global ocean and coastal waters. *Science* **359**:eaam7240.

Bukaveckas, P. A., L. E. Barry, M. J. Beckwith, V. David and B. Lederer, 2011. Factors Determining the Location of the Chlorophyll Maximum and the Fate of Algal Production within the Tidal Freshwater James River. *Estuaries and Coasts* **34**:569-582.

Caffrey, J. M., 2004. Factors controlling net ecosystem metabolism in U.S. estuaries. *Estuaries* **27**:90-101.

Caffrey, J. M., M. C. Murrell, K. S. Amacker, J. W. Harper, S. Phipps and M. S. Woodrey, 2014. Seasonal and Inter-annual Patterns in Primary Production, Respiration, and Net Ecosystem Metabolism in Three Estuaries in the Northeast Gulf of Mexico. *Estuaries and Coasts* **37**:222-241.

Cai, W.-J., 2011. Estuarine and Coastal Ocean Carbon Paradox: CO2 Sinks or Sites of Terrestrial Carbon Incineration? *Annual Review of Marine Science* **3**:123-145.

Carstensen, J., J. H. Andersen, B. G. Gustafsson and D. J. Conley, 2014. Deoxygenation of the Baltic Sea during the last century. *Proceedings of the National Academy of Sciences* **111**:5628-5633.

CBP, 2010. Chesapeake Bay TMDL Document.

Cerco, C. F. and M. R. Noel, 2013. Twenty-one-year simulation of Chesapeake Bay water quality using the CE-QUAL-ICM eutrophication model. *Journal of the American Water Resources Association*:doi: 10.1111/jawr.12107.

Cerco, C. F. and M. R. Noel, 2017. The 2017 Chesapeake Bay Water Quality and Sediment Transport Model: A Report to the US Environmental Protection Agency Chesapeake Bay Program. *In,* Editor (Editor)^(Editors). 1

US Army Engineer Research and Development Center, Vicksburg MS.

Conley, D. J., E. Bonsdorff, J. Carstensen, G. Destouni, B. G. Gustafsson, L. A. Hansson, N. N. Rabalais, M. Voss and L. Zillén, 2009. Tackling Hypoxia in the Baltic Sea: Is Engineering a Solution? *Environmental Science & Technology* **43**:3407-3411.

D'Avanzo, C. and J. N. Kremer, 1994. Diel oxygen dynamics and anoxic events in an eutrophic estuary of Waquoit Bay, Massachusetts. *Estuaries* **17**:131-139.

Di Toro, D. M., 2001. *Sediment flux modeling*. New York, Wiley-Interscience,

Ding, H. and A. J. Elmore, 2015. Spatio-temporal patterns in water surface temperature from Landsat time series data in the Chesapeake Bay, USA. *Remote Sensing of Environment* **168**:335-348.

Feng, Y., M. A. M. Friedrichs, J. Wilkin, H. Tian, Q. Yang, E. E. Hofmann, J. D. Wiggert and R. R. Hood, 2015. Chesapeake Bay nitrogen fluxes derived from a land-estuarine ocean biogeochemical modeling system: Model description, evaluation, and nitrogen budgets. *Journal of Geophysical Research: Biogeosciences* **120**:1666-1695.

Fennel, K., J. Hu, A. Laurent, M. Marta-Almeida and R. Hetland, 2013. Sensitivity of hypoxia predictions for the Northern Gulf of Mexico to sediment oxygen consumption and model nesting. *Journal of Geophysical Research: Oceans*:1-14.

Fennel, K. and J. M. Testa, 2019. Biogeochemical Controls on Coastal Hypoxia. *Annual Review of Marine Science* **11**:105-130.

Fisher, T. R., E. R. Peele, J. W. Ammerman and J. L.W. Harding, 1992. Nutrient limitation of phytoplankton in Chesapeake Bay. *Marine Ecology Progress Series* **82**:51-63.

Fitzpatrick, J. J., 2009. Assessing skill of estuarine and coastal eutrophication models for water quality managers. *Journal of Marine Systems* **76**:195-211.

Frank, J. M., F. M. Rohland, R. M. Stankelis, J. M. Lawrence, B. Bean, H. Pine and W. R. Boynton, 2002. Monitoring of Sediment Oxygen and Nutrient Exchanges in the Chester River Estuary in Support of TMDL Development. *In,* Editor (Editor)^(Editors). Report to the Maryland Department of the Environment, p. 80.

Ganju, N. K., J. M. Testa, S. E. Suttles and A. L. Aretxabaleta, 2020. Spatiotemporal variability of light attenuation and net ecosystem metabolism in a back-barrier estuary. *Ocean Science*.

Grantham, B. A., F. Chan, K. J. Nielsen, D. S. Fox, J. A. Barth, A. Huyer, J. Lubchenco and B. A. Menge, 2004. Upwelling-driven nearshore hypoxia signals ecosystem and oceanographic changes in the northeast Pacific. *Nature* **429**:749-754.

Harding, L. W., C. L. Gallegos, E. S. Perry, W. D. Miller, J. E. Adolf, M. E. Mallonee and H. W. Paerl, 2015. Long-term trends of nutrients and phytoplankton in Chesapeake Bay. *Estuaries and Coasts* **39**:664-681.

Harris, L. A., C. L. S. Hodgkins, M. C. Day, D. Austin, J. M. Testa, W. Boynton, L. Van Der Tak and N. W. Chen, 2015. Optimizing recovery of eutrophic estuaries: Impact of destratification and re-aeration on nutrient and dissolved oxygen dynamics. *Ecological Engineering* **75**:470-483.

Hitchcock, G. L., G. Kirkpatrick, P. V. Z. Lane and C. J. Langdon, 2014. Comparative diel oxygen cycles preceding and during a Karenia bloom in Sarasota Bay, Florida, USA. *Harmful Algae* **38**:95-100.

Irby, I. D. and M. A. M. Friedrichs, 2019. Evaluating Confidence in the Impact of Regulatory Nutrient Reduction on Chesapeake Bay Water Quality. *Estuaries and Coasts* **42**:16-32.

Irby, I. D., M. A. M. Friedrichs, F. Da and K. E. Hinson, 2018. The competing impacts of climate change and nutrient reductions on dissolved oxygen in Chesapeake Bay. *Biogeosciences* **15**:2649-2668.

Irby, I. D., M. A. M. Friedrichs, C. T. Friedrichs, A. J. Bever, R. R. Hood, L. W. J. Lanerolle, M. Li, L. Linker, M. E. Scully, K. Sellner, J. Shen, J. Testa, H. Wang, P. Wang and M. Xia, 2016. Challenges associated with modeling low-oxygen waters in Chesapeake Bay: A multiple model comparison. *Biogeosciences* **13**:2011-2028.

Jordan, T. E., J. C. Cornwell, W. R. Boynton and J. T. Anderson, 2008. Changes in phosphorus biogeochemistry along an estuarine salinity gradient: the iron conveyor belt. *Limnology and Oceanography* **53**:172-184.

743 Justíc, D., N. N. Rabalais and R. E. Turner, 1996. Effects of climate change on hypoxia in
744 coastal waters: A doubled CO_2 scenario for the northern Gulf of Mexico. *Limnology and*
745 *Oceanography* **41**:992-1003.
746 Justíc, D., R. E. Turner and N. N. Rabalais, 2003. Climatic influences on riverine nitrate flux:
747 Implications for coastal marine eutrophication and hypoxia. *Estuaries* **26**:1-11.
748 Kemp, W. M., W. R. Boynton, J. E. Adolf, D. F. Boesch, W. C. Boicourt, G. Brush, J. C.
749 Cornwell, T. R. Fisher, P. M. Glibert, J. D. Hagy, L. W. Harding, E. D. Houde, D. G.
750 Kimmel, W. D. Miller, R. I. E. Newell, M. R. Roman, E. M. Smith and J. C. Stevenson,
751 2005. Eutrophication of Chesapeake Bay: Historical trends and ecological interactions.
752 *Marine Ecology Progress Series* **303**:1-29.
753 Koweek, D. A., C. García-Sánchez, P. G. Brodrick, P. Gassett and K. Caldeira, 2020. Evaluating
754 hypoxia alleviation through induced downwelling. *Science of The Total Environment*
755 **719**:137334.
756 Lajaunie-Salla, K., A. Sottolichio, S. Schmidt, X. Litrico, G. Binet and G. Abril, 2018. Future
757 intensification of summer hypoxia in the tidal Garonne River (SW France) simulated by a
758 coupled hydro sedimentary-biogeochemical model. *Environmental Science and Pollution*
759 *Research* **25**:31957-31970.
760 Lake, S. J. and M. J. Brush, 2015. Modeling estuarine response to load reductions in a warmer
761 climate: the York River Estuary, Virginia, USA. *Marine Ecology Progress Series*
762 **538**:81-98.
763 Laurent, A. and K. Fennel, 2014. Simulated reduction of hypoxia in the northern Gulf of Mexico
764 due to phosphorus limitation. *Elementa*:doi: 10.12952/journal.elementa.000022.
765 Laurent, A., K. Fennel, D. S. Ko and J. Lehrter, 2018. Climate Change Projected to Exacerbate
766 Impacts of Coastal Eutrophication in the Northern Gulf of Mexico. *Journal of*
767 *Geophysical Research: Oceans* **123**:3408-3426.
768 Lefcheck, J. S., D. J. Wilcox, R. R. Murphy, S. R. Marion and R. J. Orth, 2017. Multiple
769 stressors threaten the imperiled coastal foundation species eelgrass (Zostera marina) in
770 Chesapeake Bay, USA. *Global Change Biology* **23**:3474-3483.
771 Li, M., Y.-J. Lee, J. M. Testa, Y. Li, W. Ni, W. M. Kemp and D. M. D. Toro, 2016. What drives
772 interannual variability of estuarine hypoxia: Climate forcing versus nutrient loading?
773 *Geophysical Research Letters* **43**:2127-2134.
774 McGlathery, K. J., K. Sundbäck and I. C. Anderson, 2007. Eutrophication in shallow coastal
775 bays and lagoons: the role of plants in the coastal filter. *Marine Ecology Progress Series*
776 **348**:1-18.
777 Meier, H. E. M., H. C. Andersson, K. Eilola, B. G. Gustafsson, I. Kuznetsov, B. Müller-Karulis,
778 T. Neumann and O. P. Savchuk, 2011. Hypoxia in future climates: A model ensemble
779 study for the Baltic Sea. *Geophysical Research Letters* **38**:L24608,
780 doi:24610.21029/22011GL049929.
781 Miller, D. C., R. J. Geider and H. L. MacIntyre, 1996. Microphytobenthos: the ecological role of
782 the "secret garden" of unvegetated, shallow-water marine habitats. II. Role in sediment
783 stability and shallow-water food webs. *Estuaries* **19**:202-212.
784 Murphy, G. E. P., T. N. Romanuk and B. Worm, 2020. Cascading effects of climate change on
785 plankton community structure. *Ecology and evolution* **10**:2170-2181.
786 Murphy, R. R., W. M. Kemp and W. P. Ball, 2011. Long-term trends in Chesapeake Bay
787 seasonal hypoxia, stratification, and nutrient loading. *Estuaries and Coasts* **34**:1293-
788 1309.

Murrell, M. C., J. M. Caffrey, D. T. Marcovich, M. W. Beck, B. M. Jarvis and J. D. I. Hagy, 2018. Seasonal oxygen dynamics in a warm temperate estuary: effects of hydrologic variability on measurements of primary production, respiration, and net metabolism. *Estuaries and Coasts* **41**:690-707.

Neff, R., H. Chang, C. G. Knight, R. Najjar, B. Yarnal and H. Walker, 2000. Impact of climate variation and change on Mid-Atlantic region hydrology and water resources. *Climate Research* **14**:207-218.

Ni, W., M. Li, A. C. Ross and R. G. Najjar, 2019. Large Projected Decline in Dissolved Oxygen in a Eutrophic Estuary Due to Climate Change. *Journal of Geophysical Research: Oceans* **124**:8271-8289.

Ni, W., M. Li and J. M. Testa, 2020. Discerning effects of warming, sea level rise and nutrient management on long-term hypoxia trends in Chesapeake Bay. *Science of The Total Environment* **737**:139717.

Nixon, S. W., R. W. Fulweiler, B. A. Buckley, S. L. Granger, B. L. Nowicki and K. M. Henry, 2009. The impact of changing climate on phenology, productivity, and benthic-pelagic coupling in Narragansett Bay. *Estuarine, Coastal and Shelf Science* **82**:1-18.

Odum, H. T. and C. M. Hoskin, 1958. Comparative studies of the metabolism of marine waters. *Publications of the Institute of Marine Science-University of Texas* **5**:16-46.

Ortiz-Bobea, A., H. Wang, C. M. Carrillo and T. R. Ault, 2019. Unpacking the climatic drivers of US agricultural yields. *Environmental Research Letters* **14**:064003.

Paerl, H. W., L. M. Valdes, A. R. Joyner and M. F. Piehler, 2004. Solving problems resulting from solutions: evolution of a dual nutrient management strategy for the eutrophying Neuse River Estuary, North Carolina. *Environmental Science and Technology* **38**:3068-3073.

Qin, Q. and J. Shen, 2019. Pelagic contribution to gross primary production dynamics in shallow areas of York River, VA, U.S.A. *Limnology and Oceanography* **64**:1484-1499.

Shen, C., J. M. Testa, M. Li, W.-J. Cai, G. G. Waldbusser, W. Ni, W. M. Kemp, J. C. Cornwell, B. Chen, J. Brodeur and J. Su, 2019a. Controls on Carbonate System Dynamics in a Coastal Plain Estuary: A Modeling Study. *Journal of Geophysical Research: Biogeosciences* **0**.

Shen, C., J. M. Testa, W. Ni, W.-J. Cai, M. Li and W. M. Kemp, 2019b. Ecosystem Metabolism and Carbon Balance in Chesapeake Bay: A 30-Year Analysis Using a Coupled Hydrodynamic-Biogeochemical Model. *Journal of Geophysical Research: Oceans* **124**:6141-6153.

Shenk, G. W., J. Wu and L. C. Linker, 2012. Enhanced HSPF Model Structure for Chesapeake Bay Watershed Simulation. *Journal of Environmental Engineering* **138**:949-957.

Smith, S. V., J.T. Hollibaugh, S.J. Dollar, and S. Vink, 1991. Tomales Bay metabolism C-N-P stoichiometry and ecosystem heterotrophy at the land-sea interface. *Estuarine, Coastal and Shelf Science* **33**:223-257.

Stow, C. A., J. Jolliff, D. J. McGillicuddy, S. C. Doney, J. I. Allen, M. A. M. Friedrichs, K. A. Rose and P. Wallhead, 2009. Skill assessment for coupled biological/physical models of marine systems. *Journal of Marine Systems* **76**:12-12.

Tassone, S. J. and P. A. Bukaveckas, 2019. Seasonal, Interannual, and Longitudinal Patterns in Estuarine Metabolism Derived from Diel Oxygen Data Using Multiple Computational Approaches. *Estuaries and Coasts* **42**:1032-1051.

Testa, J. M., D. C. Brady, D. M. Di Toro, W. R. Boynton, J. C. Cornwell and W. M. Kemp, 2013. Sediment flux modeling: nitrogen, phosphorus and silica cycles. *Estuarine, Coastal and Shelf Science* **131**:245-263.

Testa, J. M. and W. M. Kemp, 2008. Variability of biogeochemical processes and physical transport in a partially stratified estuary: a box-modeling analysis. *Marine Ecology Progress Series* **356**:63-79.

Testa, J. M. and W. M. Kemp, 2014. Spatial and temporal patterns in winter-spring oxygen depletion in Chesapeake Bay bottom waters. *Estuaries and Coasts* **37**:1432-1448.

Testa, J. M., W. M. Kemp, W. R. Boynton and J. D. Hagy, 2008. Long-term changes in water quality and productivity in the Patuxent River estuary: 1985 to 2003. *Estuaries and Coasts* **31**:1021-1037.

Testa, J. M., Y. Li, Y. J. Lee, M. Li, D. C. Brady, D. M. D. Toro and W. M. Kemp, 2014. Quantifying the effects of nutrient loading on dissolved O_2 cycling and hypoxia in Chesapeake Bay using a coupled hydrodynamic-biogeochemical model. *Journal of Marine Systems* **139**:139-158.

Testa, J. M., R. R. Murphy, D. C. Brady and W. M. Kemp, 2018. Nutrient- and climate-induced shifts in the phenology of linked biogeochemical cycles in a temperate estuary. *Frontiers in Marine Science*:https://doi.org/10.3389/fmars.2018.00114.

Thébault, J., T. S. Schraga, J. E. Cloern and E. G. Dunlavey, 2008. Primary production and carrying capacity of former salt ponds after reconnection to San Francisco Bay. *Wetlands* **28**:841-851.

Tian, R., 2020. Factors Controlling Hypoxia Occurrence in Estuaries, Chester River, Chesapeake Bay. *Water* **12**.

Tyler, R. M., D. C. Brady and T. Targett, 2009. Temporal and spatial dynamics of diel-cycling hypoxia in estuarine tributaries. *Estuaries and Coasts* **32**:123-145.

VIMS, 2020. Virginia Institute of Marine Sciences SAV Monitoring & Restoration; Seagrass Area by Segment.

Wagena, M. B., A. S. Collick, A. C. Ross, R. G. Najjar, B. Rau, A. R. Sommerlot, D. R. Fuka, P. J. A. Kleinman and Z. M. Easton, 2018. Impact of climate change and climate anomalies on hydrologic and biogeochemical processes in an agricultural catchment of the Chesapeake Bay watershed, USA. *Science of The Total Environment* **637-638**:1443-1454.

Wang, B., J. Hu, S. Li, L. Yu and J. Huang, 2018. Impacts of anthropogenic inputs on hypoxia and oxygen dynamics in the Pearl River estuary. *Biogeosciences* **15**:6105-6125.

Yvon-Durocher, G., J. M. Caffrey, A. Cescatti, M. Dossena, P. del Giorgio, J. M. Gasol, J. M. Montoya, J. Pumpanen, P. A. Staehr and M. Trimmer, 2012. Reconciling the temperature dependence of respiration across timescales and ecosystem types. *Nature* **487**:472.

Yvon-Durocher, G., J. I. Jones, M. Trimmer, G. Woodward and J. M. Montoya, 2010. Warming alters the metabolic balance of ecosystems. *Philosophical Transactions of the Royal Society B: Biological Sciences* **365**:2117-2126.

Zhang, Q., T. R. Fisher, E. M. Trentacoste, C. Buchanan, A. B. Gustafson, R. Karrh, R. R. Murphy, J. Keisman, C. Wu, R. Tian, J. M. Testa and P. J. Tango, 2020. An empirical approach for predicting long-term changes in nutrient limitation of phytoplankton growth in a temperate estuar.in review.

Zhang, Q., P. J. Tango, R. R. Murphy, M. K. Forsyth, R. Tian, J. Keisman and E. M. Trentacoste 2018. Chesapeake Bay Dissolved Oxygen Criterion Attainment Deficit: Three Decades of Temporal and Spatial Patterns. *Frontiers in Marine Science* **5**.

880

881

882

883

884

885

Table 1: Model performance metrics across 8 locations in the Chester river estuary, including root mean squared error (RMSE), mean error (ME), and relativity index (RI) for water-column chlorophyll-a, dissolved oxygen (DO), ammonium, nitrate+nitrite, and phosphate. For ET4.2, "S" is surface water (0.5 m) and "B" is bottom water.

Station	Metric	Chl-a $\mu g\ L^{-1}$	DO $mg\ L^{-1}$	NH_4 $mg\ L^{-1}$	NO_{23} $mg\ L^{-1}$	PO_4 $mg\ L^{-1}$
XIH4495	RMSE	7.36	1.83	0.11	0.33	0.038
Salinity = 0.2	ME	3.56	1.81	-0.06	0.05	-0.032
Depth = 2.4	RI	3.0	1.3	2.6	1.3	2.8
XIH0077	RMSE	4.81	1.22	0.11	0.73	0.042
Salinity = 3.2	ME	-2.85	0.97	0.06	0.69	-0.039
Depth = 4.8	RI	2.8	1.2	2.0	2.2	3.0
XHH7848	RMSE	10.3	1.54	0.13	0.58	0.023
Salinity = 5.2	ME	-6.22	1.20	0.06	0.55	-0.018
Depth = 4.6	RI	2.4	1.2	2.3	2.6	2.0
XHH6419	RMSE	27.84	1.46	0.14	0.43	0.018
Salinity = 6.4	ME	-16.88	-0.15	0.12	0.39	-0.007
Depth = 3.3	RI	3.5	1.2	5.0	3.2	2.9
XHG1579	RMSE	29.93	2.79	0.09	0.27	0.009
Salinity = 7.6	ME	-15.94	-1.37	0.07	0.23	0.002
Depth = 2.8	RI	2.7	1.3	5.0	4.6	3.0
ET4.2, Surface	RMSE	13.54	1.67	0.11	0.23	0.012
Salinity = 7.8	ME	-6.20	-1.03	0.03	0.15	0.002
Depth = 13.0	RI	2.2	1.2	4.1	2.3	2.9
ET4.2, Bottom	RMSE	14.87	3.45	0.16	0.28	0.015
Salinity = 10.4	ME	-7.05	0.56	0.004	0.19	-0.001
Depth = 13.0	RI	2.9	3.1	3.5	2.5	2.8

Table 2: Characteristics of stations used in model validation, sediment rate process measurements, and derived metabolic estimates and continuous water properties. Data sources included in the text.

Station Code	System	Latitude	Longitude	Depth, m	Mean Salinity	Measurement Type	Years Visited
CHE0348	Chester River	39.2403	-75.9586	1.7	0.68	Continuous Monitoring; Metabolism Estimates	2003-2006
XIH0077	Chester River	39.1666	-76.0387	3.0	4.69	Continuous Monitoring; Metabolism Estimates	2003-2006
XHH3851	Corsica River	39.0628	-76.0816	1.8	6.88	Continuous Monitoring; Metabolism Estimates	2003-2017
XHH5046	Corsica River	39.0832	-76.1073	1.9	7.81	Continuous Monitoring; Metabolism Estimates	2005-2006
XHH4931	Corsica River	39.0812	-76.1149	2.4	8.44	Continuous Monitoring; Metabolism Estimates	2006-2017
XHH4916	Corsica River	39.0818	-76.1392	4.2	8.73	Continuous Monitoring; Metabolism Estimates	2006-2011
XGG8458	Chester River	38.9734	-76.2367	0.8	10.9	Continuous Monitoring; Metabolism Estimates	2007-2009
XGG8359	Chester River	38.9713	-76.2357	0.6	11.13	Continuous Monitoring; Metabolism Estimates	2007-2009
CR01	Chester River	39.2420	-75.9482	2.8	0.20	Sediment Water Flux & Sediment Nutrients	2001
CR02	Chester River	39.2391	-76.0080	2.7	1.14	Sediment Water Flux & Sediment Nutrients	2001
CR06	Chester River	39.1652	-76.0459	2.3	5.40	Sediment Water Flux & Sediment Nutrients	2001
CRb	Corsica River	39.0786	-76.0979	2.2	8.06	Sediment Water Flux & Sediment Nutrients	2006
CR08	Chester River	39.1282	-76.0966	7.7	9.23	Sediment Water Flux & Sediment Nutrients	2001
CR09	Chester River	39.1100	-76.1277	3.5	9.48	Sediment Water Flux & Sediment Nutrients	2001
CR16	Chester River	39.1031	-76.1421	5.7	9.65	Sediment Water Flux & Sediment Nutrients	2001
CR19	Chester River	38.9989	-76.2016	6.3	11.68	Sediment Water Flux & Sediment Nutrients	2001
CR18	Chester River	39.0285	-76.1849	7.3	11.70	Sediment Water Flux & Sediment Nutrients	2001
XIH4495	Chester River	39.2387	-76.0034	2.6	0.23	Water Column Nutrients, Chl-a, TSS, Temp, Salinity	2003
ET4.1	Chester River	39.2437	-75.9249	4.4	0.54	Water Column Nutrients, Chl-a, TSS, Temp, Salinity	1984-2019
XIH0077	Chester River	39.1667	-76.0387	3.6	4.89	Water Column Nutrients, Chl-a, TSS, Temp, Salinity	2003-2006
XHH7848	Chester River	39.1298	-76.0877	7.3	5.43	Water Column Nutrients, Chl-a, TSS, Temp, Salinity	2003
XHH4822	Corsica River	39.0804	-76.1303	4.5	7.02	Water Column Nutrients, Chl-a, TSS, Temp, Salinity	2003-2005
XHH6419	Chester River	39.1076	-76.1345	3.8	7.41	Water Column Nutrients, Chl-a, TSS, Temp, Salinity	2003-2006
XHG1579	Chester River	39.0257	-76.2017	2.6	8.50	Water Column Nutrients, Chl-a, TSS, Temp, Salinity	2003-2006
CB3.2	Chesapeake Bay	39.1637	-76.3063	12.5	9.47	Water Column Nutrients, Chl-a, TSS, Temp, Salinity	1984-2019
CB3.3E	Chesapeake Bay	39.0041	-76.3452	8.0	10.08	Water Column Nutrients, Chl-a, TSS, Temp, Salinity	1984-2019
ET4.2	Chester River	38.9923	-76.2151	15.0	10.47	Water Column Nutrients, Chl-a, TSS, Temp, Salinity	1984-2019

Figure 1: Location of Chester River Estuary on the northeastern shore of the Chesapeake Bay (left panel), bathymetry of the Chester river estuary with grid location and freshwater sources (top right panel), and maximum depth distribution along the central channel of the Chester River within the model domain.

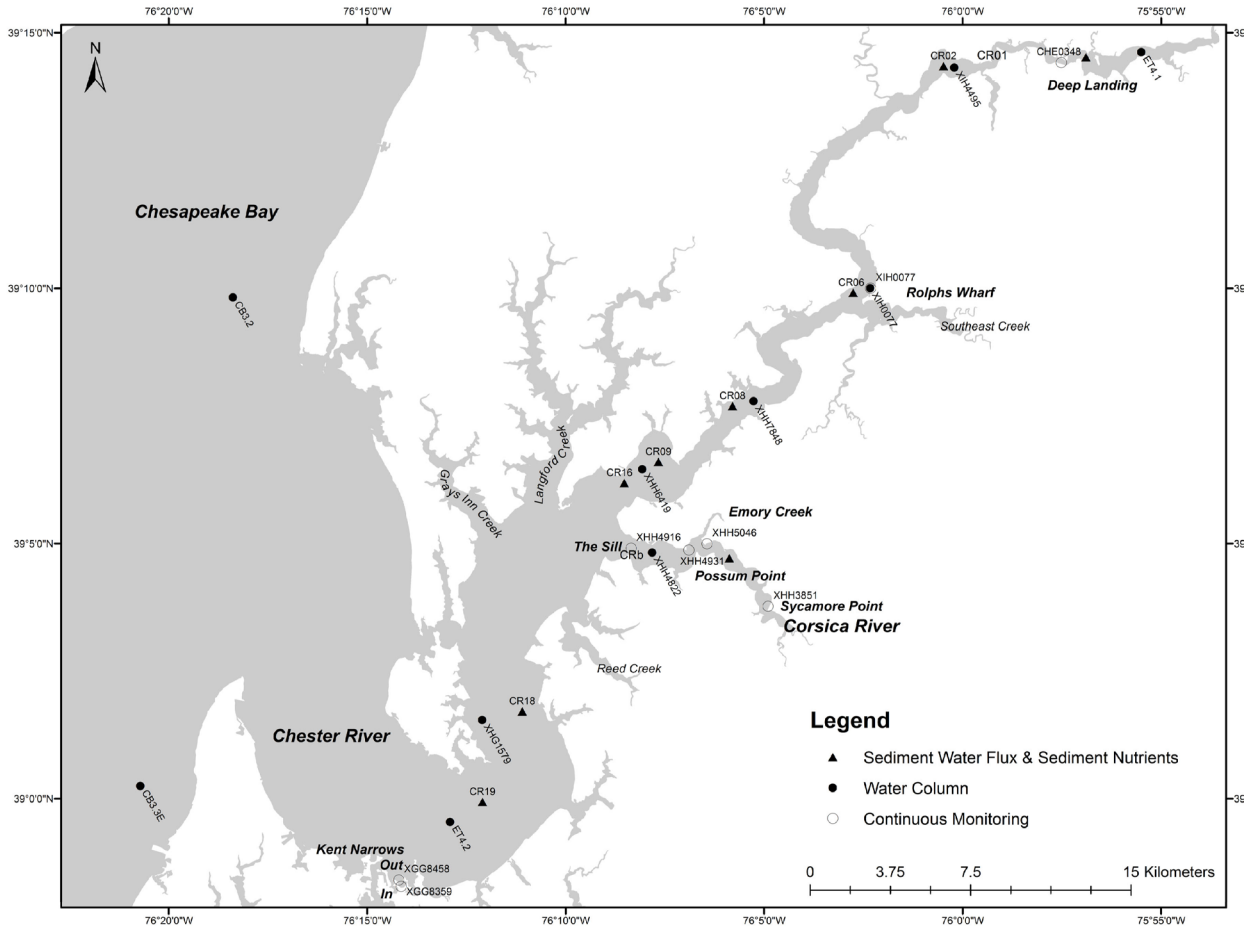

Figure 2: Map of water-column and sediment process and concentration measurement and monitoring stations in the Chester River estuary. See Table 2 for station location and measurement types. These include sediment-water flux and sediment nutrients content (triangles) stations, Chesapeake Bay Program (CBP) long-term water quality monitoring stations (ET4.1 and ET4.2; closed circles), continuous sensor deployment stations (open circles), and short-term biogeochemical monitoring stations (closed circles).

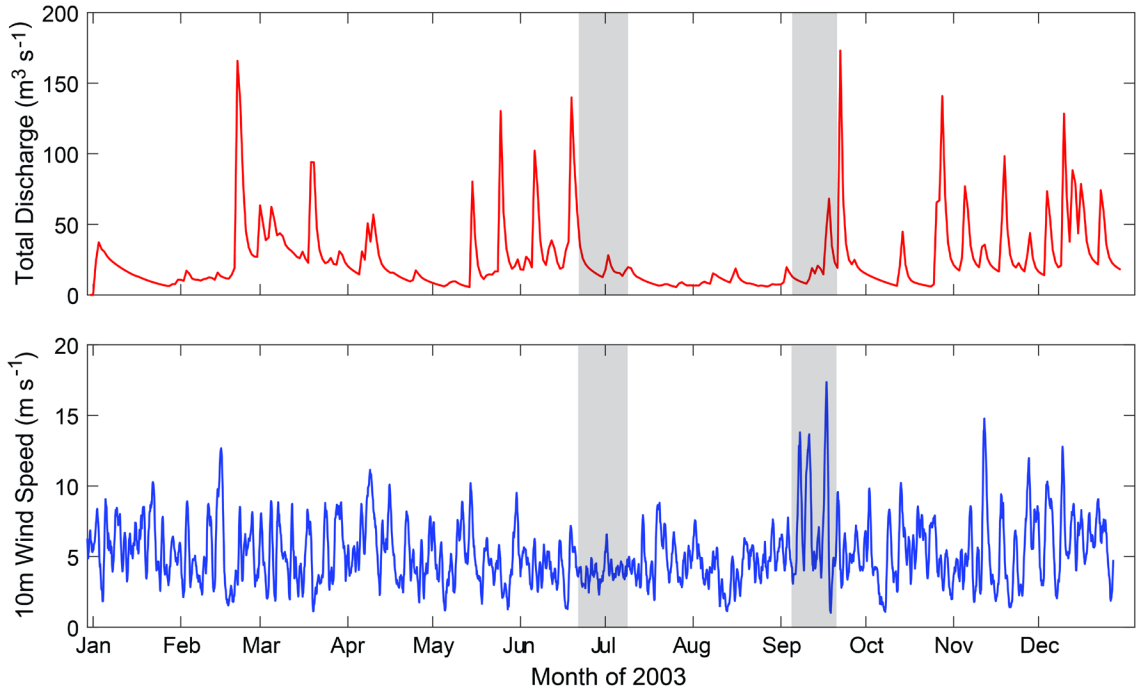

Figure 3: Annual hydrograph of total freshwater discharge into the Chester River (top) and local wind speed derived in 2003. Shaded periods in the top and bottom panels highlight two periods where oxygen was depressed below 4 mg/L at a shallow-water location within the Chester River estuary (see Fig. 12).

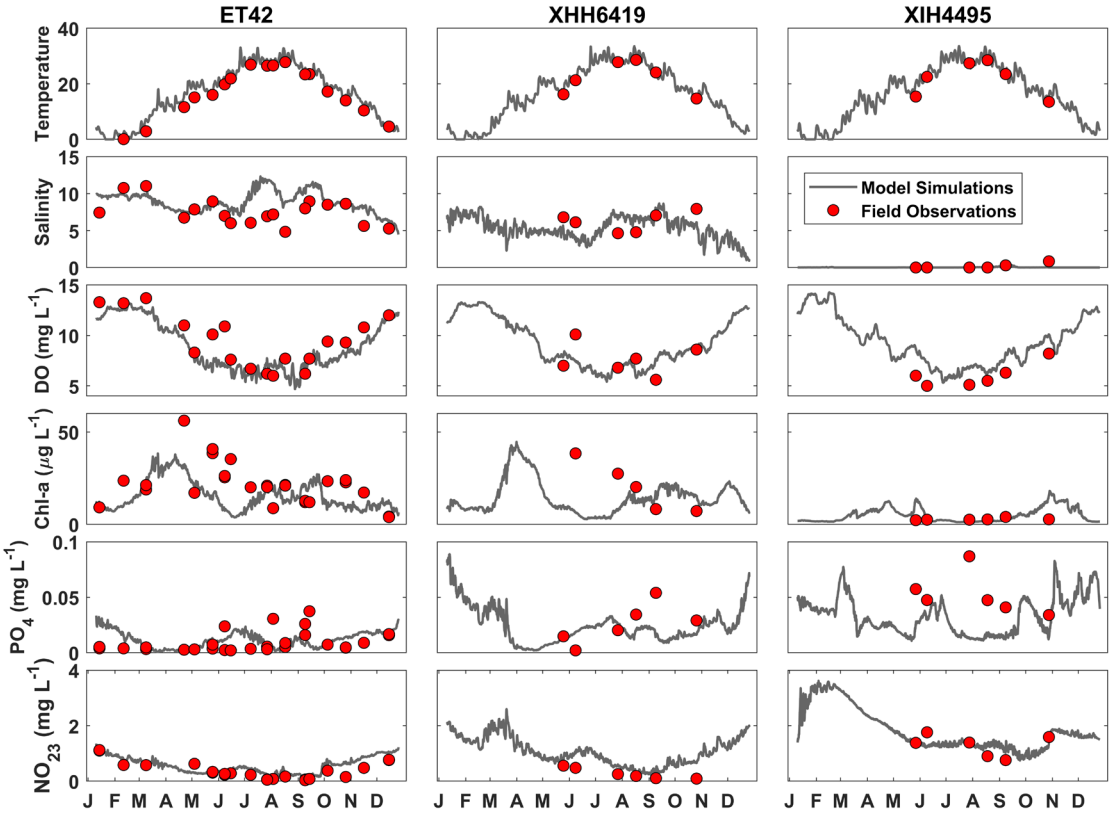

Figure 4: Comparisons of model-simulated (lines) and observed (closed circles) surface water properties at three stations oriented along the channel of the Chester River estuary, including water-temperature, salinity, dissolved oxygen (DO), chlorophyll-a, phosphate, and nitrate+nitrite (see Figure 2 for station locations).

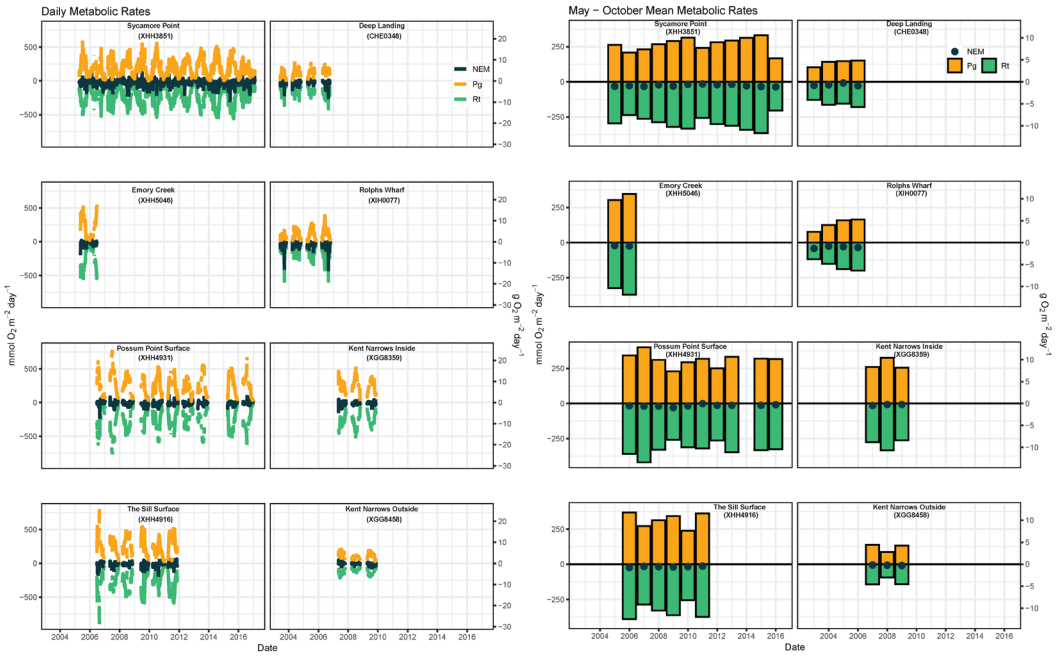

Figure 5: Daily (left) and May-October average (right) rates of Pg, Rt, and NEM derived from continuous oxygen time-series across eight stations in the Chester River Estuary. Computations made using approach of Beck et al. (2015). For each time period, left panels are Corsica River sub-tributary stations (Sycamore Point, Emory Creek, Possum Point, The Sill) and right panels are in the main Chester River body (Deep Landing, Rolphs Wharf, Kent Narrows Inside and Outside). Salinity increases from top to bottom (see Figure 2 and Table 2 for station details).

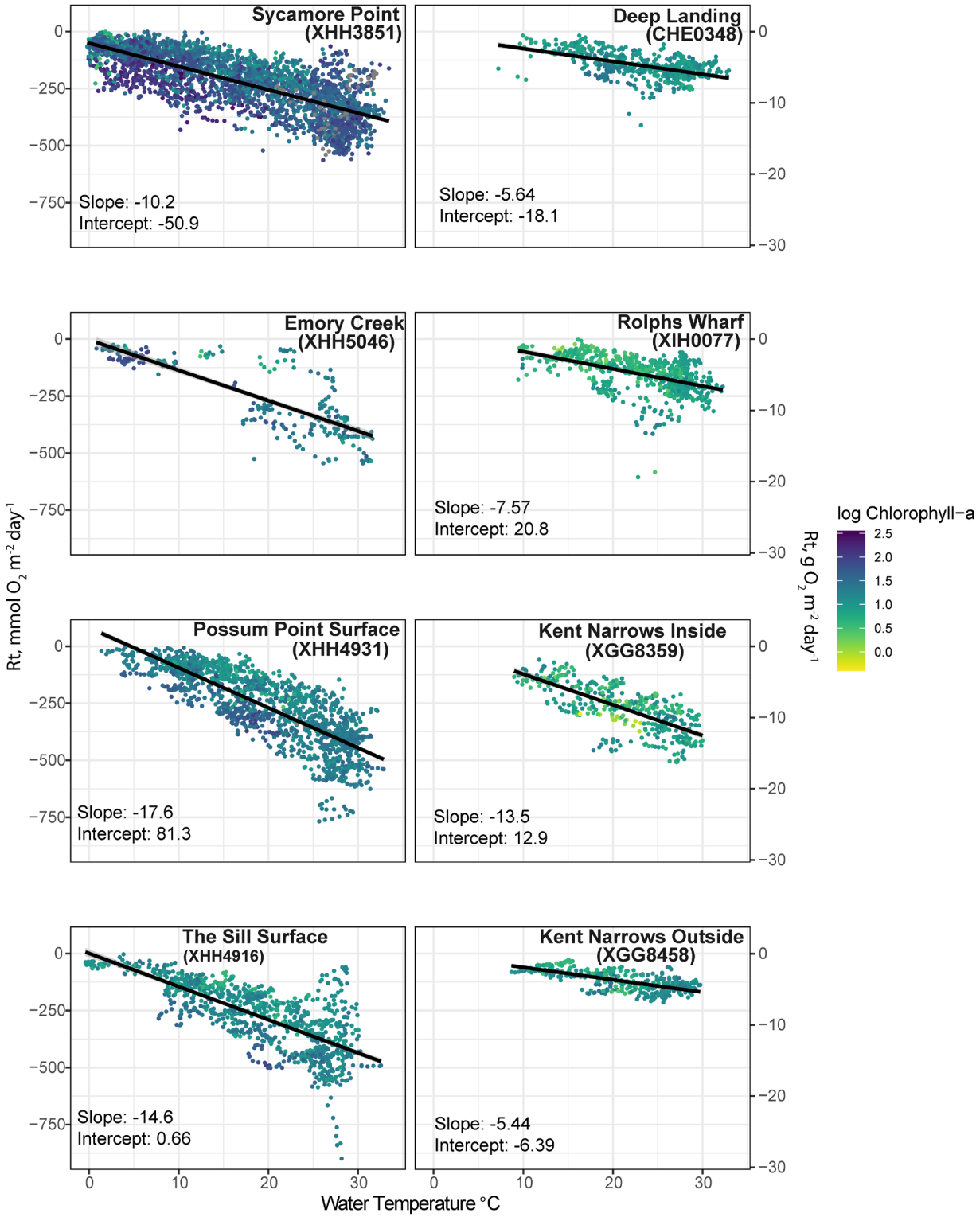

Figure 6: Relationships between daily water temperature and daily rates of ecosystem respiration derived from dissolved oxygen time series. Color of circles represents mean daily log

chlorophyll-a. Rt is a rate of oxygen uptake, where increasingly negative values indicate higher respiration. For each regression, the slope and intercept (in units of mmol O_2 m^{-2} d^{-1}) are included. See Figure 2 and Table 2 for station information and location.

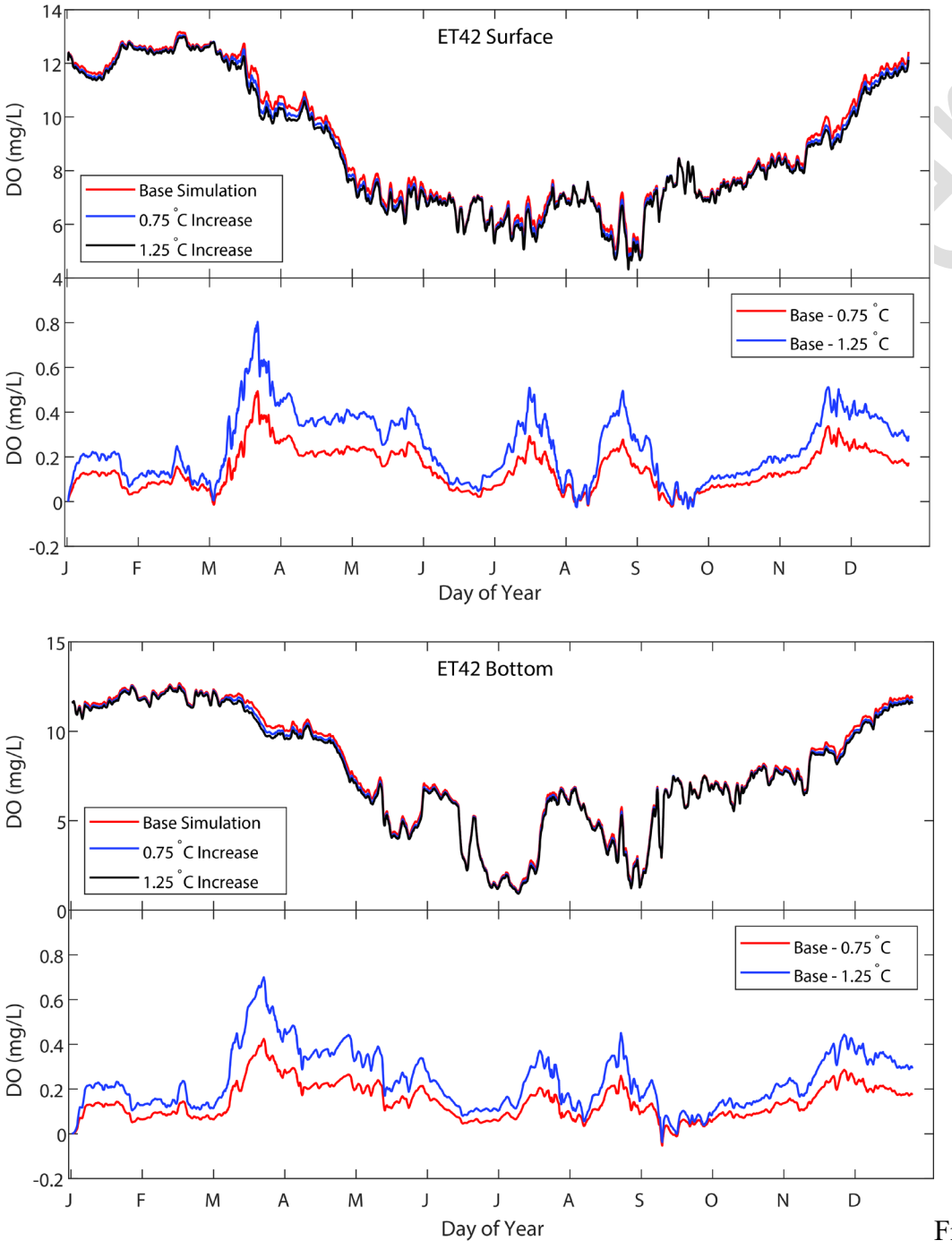

Figure 7: Model-simulated dissolved oxygen concentrations and deviations from the baseline simulation under warming (Base-degree increase) in surface (top panels) and bottom waters (bottom panels) in the region of ET4.2 in 2003.

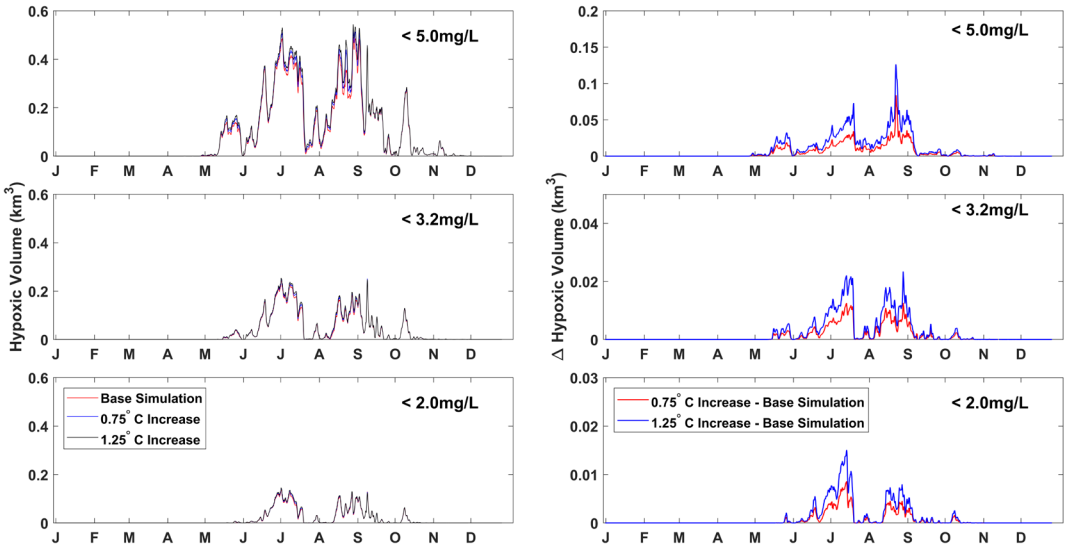

Figure 8: Time-series of model-computed volumes of low-oxygen water across the entire Chester River estuary computed below multiple thresholds (< 5, 3.2, and 2 mg O_2 L^{-1}) under baseline scenarios and under warming of 0.75 ºC and 1.25 ºC (left panels) and differences (Δ Hypoxic Volume) between warming scenarios and the baseline simulation in the Chester River (right panels).

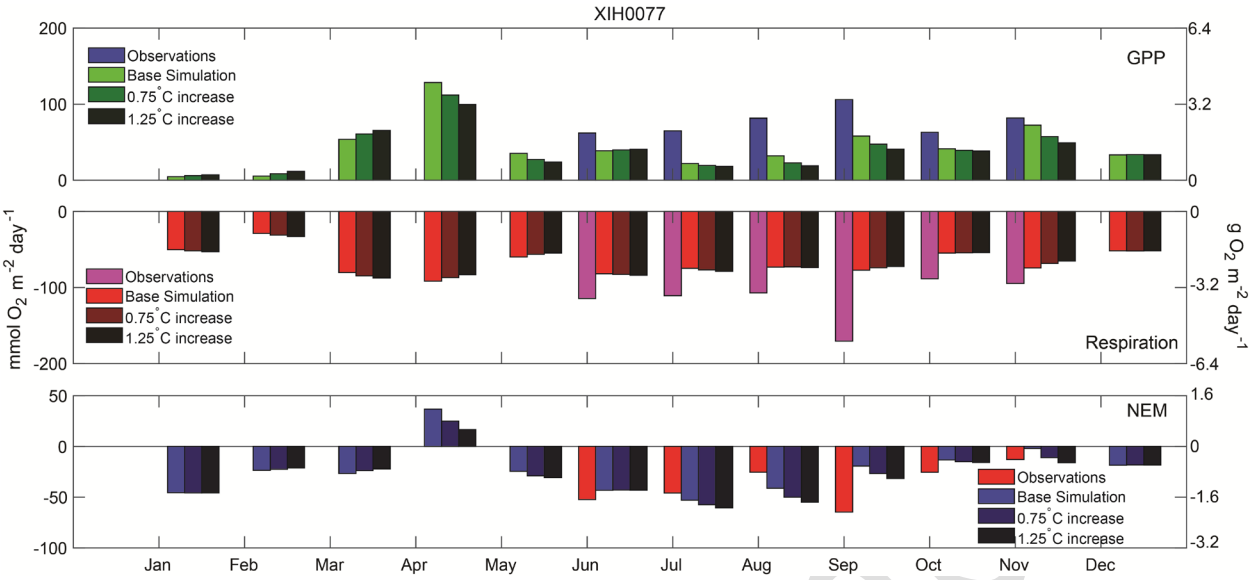

Figure 9: Monthly mean modeled and derived rates of water-column and sediment integrated gross primary production (GPP; top panel), respiration (Resp middle panel), and net ecosystem metabolism (NEM; bottom panel) at station XIH0077 (see Figure 2). Modeled rates include the 2003 simulation and warming simulations with +0.75 and +1.25 ºC.

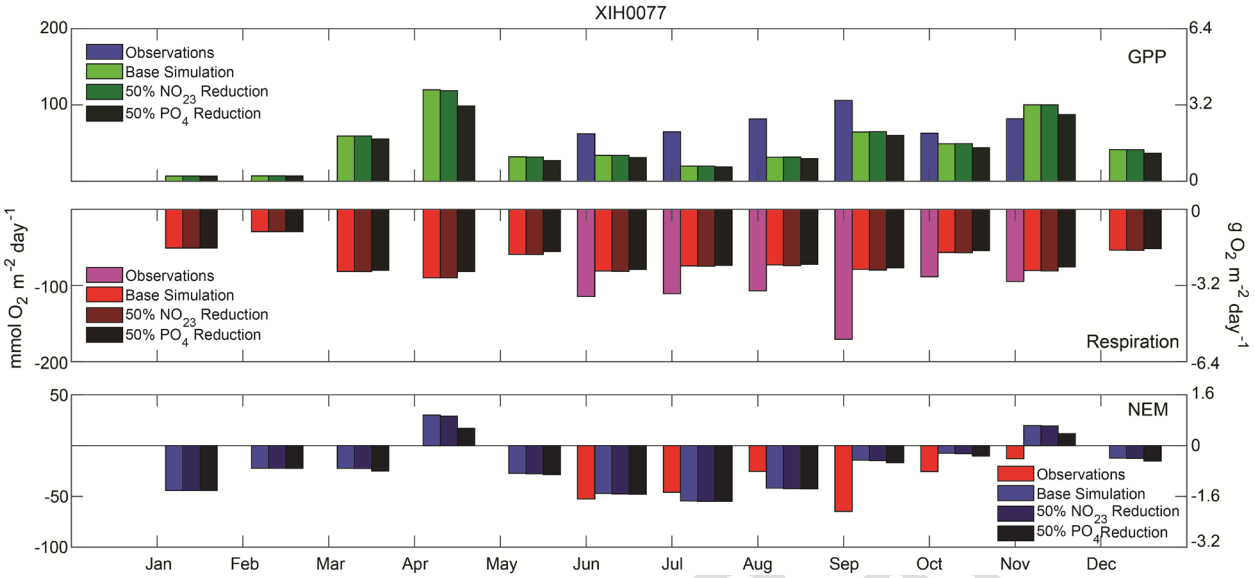

Figure 10: Monthly mean modeled and derived rates of water-column and sediment integrated gross primary production (GPP; top panel), respiration (Resp; middle panel), and net ecosystem metabolism (NEM; bottom panel) at station XIH0077 (see Figure 2). Modeled rates include the 2003 simulation and scenarios with a 50% reduction in nitrate (NO_{23}) and phosphate (PO_4) loading.

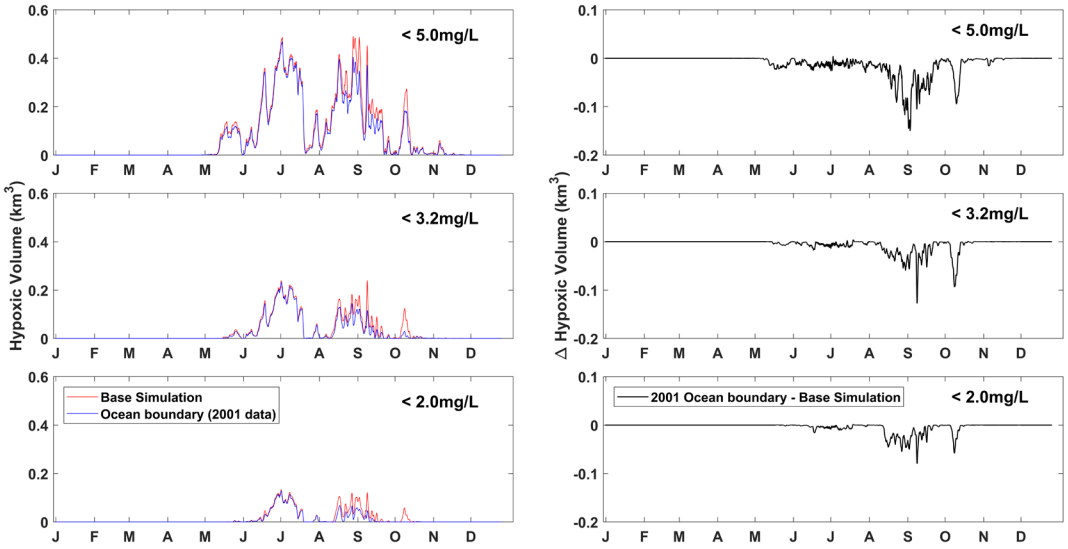

Figure 11: Time-series of model-computed volumes of low-oxygen water computed across the entire Chester River estuary below multiple thresholds (< 5, 3.2, and 2mg O_2 L^{-1}) under baseline scenarios and with open-water boundary conditions based on 2001 in Chesapeake Bay (left panels) and differences (Δ Hypoxic Volume)between the altered boundary scenario and the baseline simulation (right panels) in the Chester River.

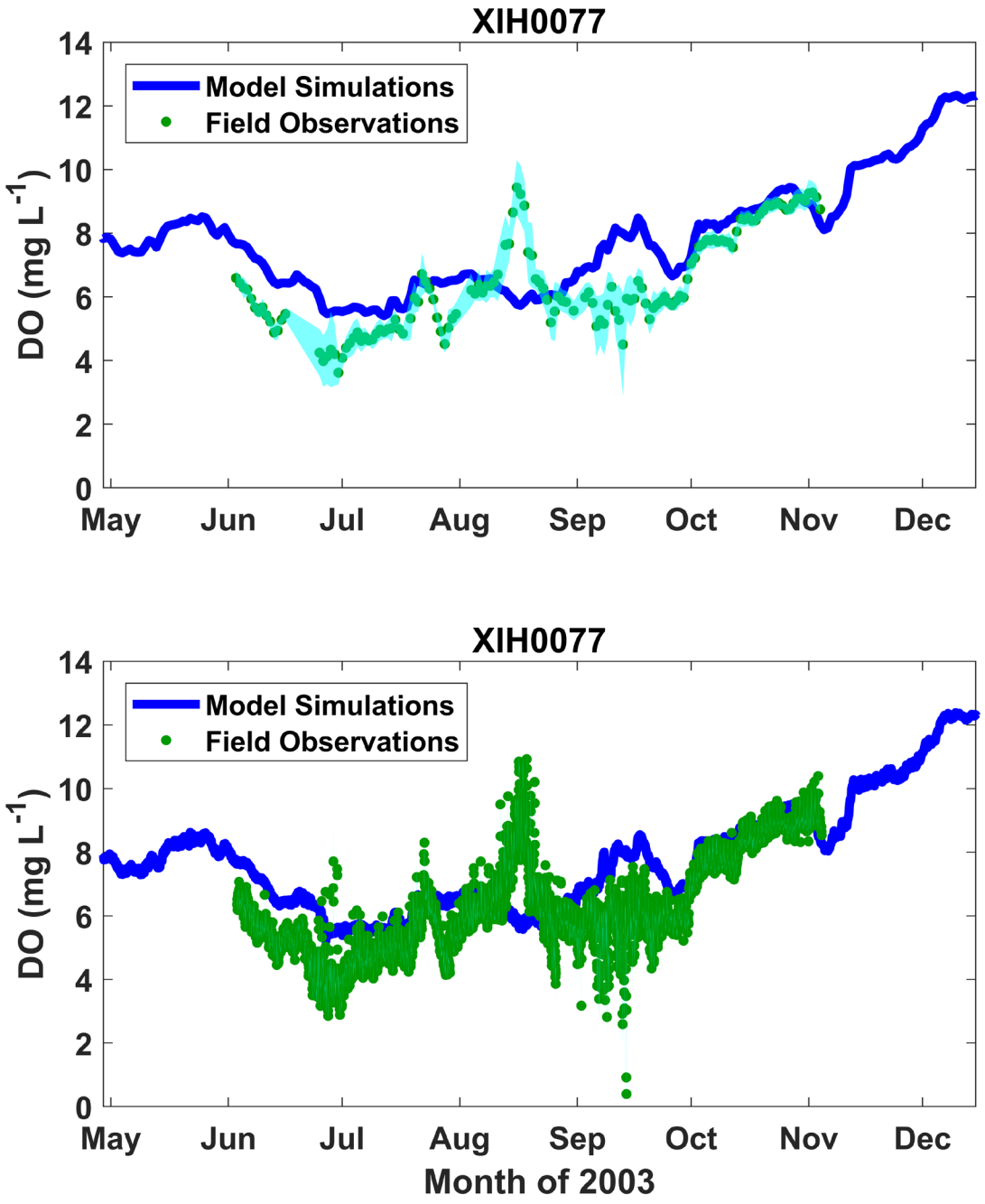

Figure 12: Comparisons of modeled (dark blue lines) and observed (green circles) oxygen concentrations at station XIH0077 (see Figure 2). The top panel includes modeled and observed oxygen values averaged over each 24 hour day (where light blue lines are 24-hour standard deviation of observations) and the bottom panel is hourly mean modeled and observed oxygen concentrations. Oxygen concentrations at XIH0077 were measured by in-situ sensors every 15-minutes from 1 meter below the surface.